Lithos 184–187 (2014) 243–258

Contents lists available at ScienceDirect

Lithos

journal homepage: www.elsevier.com/locate/lithos

Invited review article

A two-component mantle source feeding Mt. Etna magmatism: Insights from the geochemistry of primitive magmas

Alessandra Correale [a,*], Antonio Paonita [a], Mauro Martelli [a], Andrea Rizzo [a], Silvio G. Rotolo [a,b], Rosa Anna Corsaro [c], Valeria Di Renzo [d]

[a] Istituto Nazionale di Geofisica e Vulcanologia, Sezione di Palermo, via Ugo la Malfa 153, Palermo 90146, Italy
[b] Dipartimento di Scienze della Terra e del Mare (DiSTeM), Università degli Studi di Palermo, via Archirafi 36, Palermo 90123, Italy
[c] Istituto Nazionale di Geofisica e Vulcanologia, Sezione di Catania, piazza Roma 2, Catania 95123, Italy
[d] Dipartimento di Ingegneria Civile, Seconda Università degli Studi di Napoli, Real Casa dell'Annunziata, Via Roma 29, 81031 Aversa (CE), Italy

ARTICLE INFO

Article history:
Received 28 March 2013
Accepted 23 October 2013
Available online 9 November 2013

Keywords:
Mt. Etna
Hyblean Plateaux
Primitive magma
Mantle metasomatism
Peridotite
Pyroxenite

ABSTRACT

The major elements, trace elements and Sr and Nd isotopes of selected Etnean primitive rocks (<15 ky BP) were studied in order to characterize their mantle source. The noble-gas geochemistry of fluid inclusions in minerals from the same lavas was also investigated. The major element compositions of whole rocks and minerals showed that these products are among the most primitive at Mt. Etna, comprising 6.3–17.5 wt.% MgO. The variable LREE (Light Rare Earth Elements) enrichment relative to MORB (Mid-Ocean Ridge Basalt) (La_n/Yb_n = 11–26), together with the patterns of certain trace-element ratios (i.e., Ce/Yb versus Zr/Nb and Th/Y versus La/Yb), can be attributed to varying degrees of melting of a common mantle source. Numerical simulations performed with the MELTS program allowed the melting percentages associated with each product to be estimated. This led us to recalculate the hypothetical parental trace-element content of the Etnean mantle source, which was common to all of the investigated rocks. The characteristics of the Sr, Nd and He isotopes confirmed the primitive nature of the rocks, with the most-depleted and primitive lava being that of Mt. Spagnolo (SPA; $^{143}Nd/^{144}Nd$ = 0.512908 $^{87}Sr/^{86}Sr$ = 0.703317–0.703325 and $^{3}He/^{4}He$ = 7.6 Ra), and highlighted the similarity of the mantle sources feeding the volcanic activity of Mt. Etna and the Hyblean Plateau (a region to the south of Mt. Etna and characterized by older magmatism than Mt. Etna). The coupling of noble gases and trace elements suggests an origin for the investigated Etnean lavas from melting of a Hyblean-like mantle, consisting of a two-component source where a peridotitic matrix is veined by 10% pyroxenite. A variable degree of mantle contamination by crustal-like fluids, probably related to subduction, is proposed to explain the higher Sr-isotope and lower Nd-isotope values in some rocks ($^{143}Nd/^{144}Nd$ up to 0.512865 and $^{87}Sr/^{86}Sr$ up to 0.703707). This process probably occurred in the source prior to magma generation, refertilizing some portions of the mantle. Accordingly, the estimated degree of melting responsible for each magma appears to be related to its $^{87}Sr/^{86}Sr$ enrichment. In contrast, the decoupling between $^{3}He/^{4}He$ and $^{87}Sr/^{86}Sr$ ratios requires the occurrence in the crustal reservoirs of further processes capable of shifting the He isotope ratio towards slightly more radiogenic values, such as magma aging or a contribution of shallow fluid. Therefore, different residence times in the Etnean reservoir and/or various rates of magma ascent could be key parameters for preserving the original He isotope marker of the Etnean mantle source.

Contents

* Corresponding author at: Istituto Nazionale di Geofisica e Vulcanologia, via Ugo la Malfa 153, Palermo 90146, Italy. Tel.: +39 91 6809273; fax: +39 9 6809449.
E-mail address: a.correale@pa.ingv.it (A. Correale).

0024-4937/$ – see front matter © 2013 Published by Elsevier B.V.
http://dx.doi.org/10.1016/j.lithos.2013.10.038

1. Introduction

Mt. Etna in Italy is a composite stratovolcano located on the eastern coast of Sicily. It formed at the convergence zone of the European and African tectonic plates in an unusual geodynamic context characterized by subduction of the Ionian oceanic slab (Fig. 1). It may be responsible for the arc volcanism of the Aeolian archipelago (less than 100 km north of Mt. Etna) and the Triassic to Quaternary alkaline/tholeiitic mafic magmatism of the Hyblean Plateau (less than 50 km south of Mt. Etna).

In attempts to determine the origin of Etnean magmatism, several researchers have investigated the characteristics of its mantle source and possible relationships with the complex geodynamic framework (e.g., Doglioni et al., 2001; Peccerillo, 2005, and references therein). The petrological and geochemical features of the erupted products show a large variability that has led to several hypotheses about the magma origin. Many authors (e.g., Armienti et al., 2004; Carter and Civetta, 1977; Tanguy et al., 1997; Tonarini et al., 2001; Viccaro and Cristofolini, 2008; Viccaro et al., 2011, and references therein) have identified the mantle source as the main cause of the compositional and isotope variations in some Etnean lavas. A few authors (e.g., Tanguy, 1980; Tanguy et al., 1997) invoked the hypothesis of different degrees of partial melting of a homogeneous mantle source, with the existence of such a source being supported by the constant $\delta^{18}O$ (5.4 ± 0.3‰) and $^3He/^4He$ ratio ($^3He/^4He = 6.7 \pm 0.4$ Ra) measured by Marty et al. (1994) and Nuccio et al. (2008) in a wide range of Etnean volcanic rocks. In contrast, other authors (e.g., Armienti et al., 2004; Tonarini et al., 2001; Viccaro and Cristofolini, 2008; Viccaro et al., 2011) have favored a heterogeneous and metasomatized source that is closely related to the complex geodynamic context. Shallow contamination of Etnean magmas due to assimilation of rocks from the sedimentary basement and/or crustal fluids has also been suggested (e.g., Armienti et al., 2004; Michaud, 1995; Tonarini et al., 2001).

Many studies have focused on source-related issues, and some aspects are still widely debated. A central aspect has been the relationship between the mantle sources feeding Etnean and Hyblean volcanic activities, given the proximity of the two volcanic regions and the temporal continuity between them (Cadoux et al., 2007; Carter and Civetta, 1977). Although the geochemical and isotope compositions of Etnean products are slightly less depleted than Hyblean ones (Bianchini et al., 2010; Perinelli et al., 2008), there is a general similarity among the geochemical characteristics of the two areas. An understanding of Etnean petrological and geochemical characteristics may therefore be obtained from recent studies that have focused on mantle xenoliths occurring in mafic magmas of the Hyblean Plateau, that are completely lacking at Mt. Etna. By investigating Hyblean xenoliths, Correale et al. (2012) provided evidence that the local lithosphere is heterogeneous and features a shallow peridotitic layer with a tendency towards HIMU-like compositions ($^3He/^4He$ ~7 Ra, $^{143}Nd/^{144}Nd$ ~0.5129 and Zr/Nb ~4) and a pyroxenitic layer showing characteristics more similar to a DM (Depleted Mantle) source ($^3He/^4He$ ~7.6 Ra, $^{143}Nd/^{144}Nd$ ~0.5130 and Zr/Nb ~30). Given these constraints the pyroxenites could be produced by crystallization of primitive melts coming from great depth and permeating the peridotitic mantle to different levels, thus representing the metasomatic agent (Correale et al., 2012; Sapienza and Scribano, 2000).

In this paper we provide additional constraints on the mantle source of Etnean magmas by studying the products from some key eruptions that occurred during prehistorical to historical periods. They include tephra of explosive eruptions and low-volume lava flows, which have been fed by the most-primitive magmas of those erupted at Mt. Etna (MgO = 6.3–17.6 wt.%). We have integrated the following diverse approaches: (i) petrology of whole rocks, including mineral chemistry, major and trace elements, and Sr and Nd isotopes of lavas/pyroclasts, (ii) geochemistry of noble gases, including determinations of He, Ne and Ar isotopes extracted from fluid inclusions within olivine and clinopyroxene phenocrysts, and (iii) modeling of the Etnean mantle

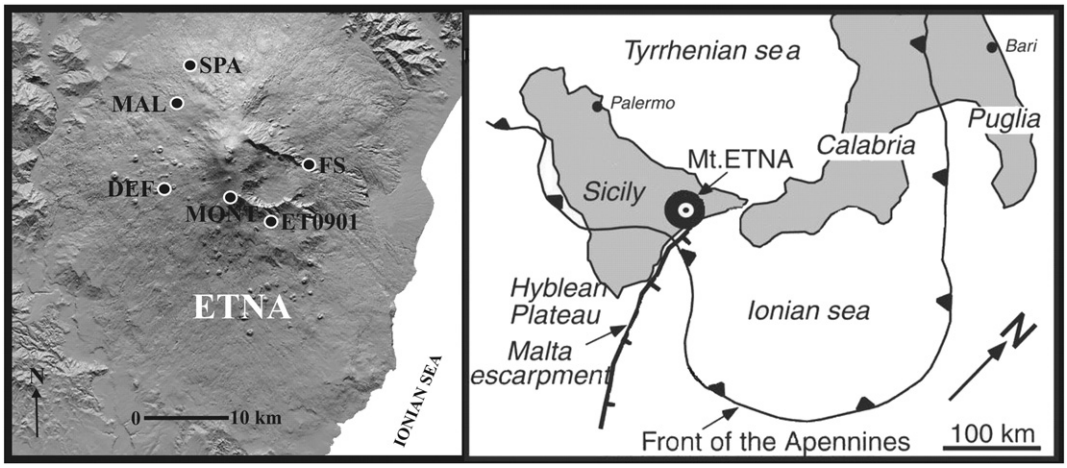

Fig. 1. Sketch map of Mt. Etna showing the sampling sites of the studied products (modified from Patanè et al., 2006) (left) and geodynamic draft of the South Italy area (modified from Doglioni et al., 2001) (right).

source, starting from the compositions of the primitive studied products and tracing back the effects of partial melting and shallow crystallization.

Our results present a more-complete picture of the features of the mantle beneath Mt. Etna, thereby providing insights into the processes controlling the generation of primitive magmas and allowing comparison with the Hyblean mantle source.

2. Summary of the geological and volcanological background

Volcanic activity at Mt. Etna began about 500 ky BP, with the Basal Tholeiitic Supersynthem (Branca et al., 2011a; De Beni et al., 2011) and eruption of submarine/subaerial tholeiitic lavas that crop out near the Ionian coast (Corsaro and Cristofolini, 1997, 2000). This was followed by the Timpe Supersynthem (220–120 ky BP; Branca et al., 2011a), which was characterized by eruptions that gradually changed from subalkaline to Na-alkaline (Corsaro and Pompilio, 2004; Tanguy, 1978). The volcanism moved westward during the next period (the Valle del Bove Supersynthem, 110–65 ky BP; Branca et al., 2011a), building several monogenetic volcanoes whose remnants are now exposed in the Valle del Bove scars (Spence and Downes, 2011). The serial affinity of the erupted magmas was distinctly Na-alkaline. The last period of activity was the Stratovolcano Supersynthem (60–2 ky BP), which was characterized by the construction of a stratovolcano in a position approximately coincident with the present-day volcano. This period can be further subdivided into the Ellittico volcano (60–15 ky BP) and the Mongibello volcano (15 ky BP to the present day). The Ellittico volcano erupted lavas and pyroclastic rocks of Na-alkaline affinity and ended its activity with four Plinian eruptions that generated pumice fall deposits and a small volume ignimbrite (Coltelli et al., 2000) related to the summit collapse of the Ellittico caldera at 15 ky BP (Branca et al., 2011a). Post-Ellittico activity continued filling the small caldera and building the Mongibello volcano. This period was dominated by eruption of lava flows and a few highly explosive eruptions (Plinian to sub-Plinian) fed by basaltic to picritic magmas (Coltelli et al., 2000, 2005). The most violent event was the basaltic Plinian eruption of 122 BC (Coltelli et al., 1998), which is associated with the formation of the Cratere del Piano summit caldera that is nested close to the older Ellittico caldera.

Activity since 122 BC is characterized by a gradual increase in the eruption frequency and an increase in K and $^{87}Sr/^{86}Sr$ isotopic ratios, especially for the magmas erupted after 1971, which is a benchmark year in the geochemistry of recent magmatism at Mt. Etna (Armienti et al., 2004; Métrich et al., 2004; Tanguy et al., 1997; Viccaro and Cristofolini, 2008).

During the last few centuries, magma has erupted from both summit craters and parasitic cones on the volcano flanks. Both “summit” and “flank” eruptions are primarily controlled by magma ascent from the central-conduits feeding system. Erupted lavas are generally K-trachybasalts that are highly porphyritic (30–40% phenocrysts) and rich in plagioclase (Armienti et al., 1988; Corsaro et al., 2009). However, a few rare flank eruptions of Mt. Etna are highly explosive and formed of nearly aphyric (5–10% phenocrysts) basaltic–trachybasaltic magma with scarce plagioclase. Such eruptions were originally termed “eccentric” (Rittman, 1965) and more recently as “deep dike fed” (DDF; Corsaro et al., 2009), a name that is free from topographical implications (i.e., eccentric relative to the summit craters) and better identifies their main characteristic—supplied by intrusions that originate from below the volcanic pile and that have apparently bypassed the central-conduit system. Historic DDF eruptions occurred in 1763 from the “La Montagnola” cone (MONT), in 1974 [Mts. De Fiore (DEF)], and in 2001 and 2002–2003 (Coulson et al., 2011). Prehistoric lavas erupted at several parasitic cones [i.e., Mt. Maletto (MAL) and SPA] could be also perhaps related to old DDF-type eruptions (Armienti et al., 1988). The occurrence of an even-more-primitive picritic magma at Mt. Etna is indicated by the fall-stratified (FS) pyroclastic deposit reported by Coltelli et al. (2005).

3. Samples and analytical methods

The samples investigated here consist of six picritic to trachybasaltic lavas and tephra from parasitic cones (Fig. 1) as follows:

1. Lava from 1974 eruption of DEF (Corsaro et al., 2009, and references therein).
2. Lava from 1763 eruption of MONT (Miraglia, 2002; Sturiale, 1970).
3. Lavas from eruptions of MAL and SPA (Armienti et al., 1988; Kamenetsky and Clocchiatti, 1996), which occurred after the Ellittico caldera collapse (15 ky BP) but before the FS lithohorizon (3930 ± 60 y BP; Branca et al., 2011b).
4. Tephra FS sample, which is from highly vesiculated (voids = 60 vol.%) scoria lapilli from the sub-Plinian FS eruption (3930 ± 60 y BP; Coltelli et al., 2005) fed by volatile-rich picritic magma that rapidly ascended from the source zone (Kamenetsky et al., 2007).
5. Tephra ET0901 sample, highly vesiculated (voids = 50 vol.%) scoria lapilli, is basanitic in composition and lies just above the FS tephra and below the FG layer (122 BC; Del Carlo et al., 2004). This scoria probably derives from a Strombolian flank eruption from the Salto del Cane parasitic cone dated as 3 ky old (Del Carlo et al., 2004).

Whole-rock composition of major elements in the investigated samples was determined by inductively coupled plasma (ICP) optical emission spectrometry at the Centre de Recherches Pétrographiques et Géochimiques in Nancy, France. Analytical uncertainty (1σ) was <1% for SiO_2 and Al_2O_3, <2% for Fe_2O_3, MgO and CaO, <5% for Na_2O, K_2O, MnO and TiO_2, and <10% for P_2O_5. For further information on the analyses see http://helium.crpg.cnrs-nancy.fr/SARM/index.html.

Trace elements were analyzed by an Agilent 7500 ICP mass spectrometer at Istituto Nazionale di Geofisica e Vulcanologia (INGV), Sezione di Palermo. Selected portions of samples were crushed and powdered with an agate mortar, then a weighed aliquot (~100 mg) was digested using HF and HNO_3. The analytical precision was ≤10% for all trace elements, while the accuracy of the method was ≤4%.

Mineral phases were analyzed with an Oxford LEO scanning electron microscopy–energy dispersive spectrometry device (housed at DISTeM, University of Palermo) using natural (standard Oxford silicate minerals) and synthetic standards for semi-quantitative analyses (Rotolo et al., 2006). An accelerating voltage of 20 kV and a beam current of 600 pA were used. Routine daily analyses on a standard glass resulted in an analytical uncertainty (1σ) of <1% for SiO_2 and Al_2O_3 and <6% for FeO, MgO, CaO, Na_2O and K_2O.

$^{87}Sr/^{86}Sr$ and $^{143}Nd/^{144}Nd$ ratios were determined in whole-rock samples and were measured by thermal-ionization mass spectrometry at the Isotope Geochemistry Laboratory of INGV, Osservatorio Vesuviano, by a TRITON TI multicollector mass spectrometer. All Sr and Nd isotopic data have been normalized to the accepted values of $^{87}Sr/^{86}Sr = 0.71025$ for the NIST-SRM 987 standard and of $^{143}Nd/^{144}Nd = 0.51185$ for the La Jolla standard, respectively. The techniques used are described by Di Renzo et al. (2007). Sr and Nd measurements were normalized for mass fractionation to $^{86}Sr/^{88}Sr = 0.1194$ and $^{146}Nd/^{144}Nd = 0.7219$, respectively. The mean measured value of $^{87}Sr/^{86}Sr$ for NIST-SRM 987 was 0.710215 ($2\sigma = 0.000011$, $N = 54$) and of $^{143}Nd/^{144}Nd$ for the La Jolla standard was 0.511841 ($2\sigma = 0.000015$, $N = 16$). The external reproducibility (2σ) value was calculated according to Goldstein et al. (2003). The Sr and Nd blanks were negligible for the analyzed samples during the period of measurements. Two distinct analyses of Sr isotopic compositions are also reported for a few of the samples.

Noble gases (He, Ne and Ar) were analyzed at INGV, Sezione di Palermo, by single-step crushing under ultra-high-vacuum conditions at a pressure of about 200 MPa. About 1–2 g of fresh olivine or pyroxene phenocrysts was hand-picked from each rock and analyzed twice. Gas

released from crushed minerals was cleaned in an appropriate preparation line connected to the mass spectrometers. He and Ne were analyzed by a Helix-SFT device, while Ar was analyzed by an Argus machine. We adopted the procedure described in Correale et al. (2012) and Nuccio et al. (2008).

4. Petrography and mineral chemistry

The main petrographic features and mineral chemistry of study rocks are summarized in Supplementary Table A1.

4.1. Lavas

Lava flows at MONT, DEF, MAL and SPA are all nearly aphyric (phenocrysts ≤15 vol.%), distinctly poorer in crystals than the Etnean trachybasalts fed by the central-conduits system, which are typically rich in crystals (phenocrysts up to 50 vol.%; Corsaro and Pompilio, 2004).

Phenocrysts are set in a microcrystalline matrix and consist of euhedral to subhedral olivine (up to 2 mm in length), which is more abundant than clinopyroxene (subhedral, up to 3 mm in length), and titaniferous magnetite. The microlitic constituents of the groundmass are: plagioclase > clinopyroxene ≥ olivine ≥ Ti-magnetite.

The forsterite content of olivine phenocrysts (Table A1) is Fo_{85-91} for MAL, Fo_{74-89} for SPA, Fo_{71-81} for MONT and Fo_{75-83} for DEF. Clinopyroxene phenocrysts are $Wo_{44-47}En_{29-37}Fs_{4-9}$ for DEF, $Wo_{40-46}En_{36-42}Fs_{3-7}$ for SPA, $Wo_{38-44}En_{36-43}Fs_{7-12}$ for MAL and $Wo_{45-48}En_{29-38}Fs_{6-11}$ for MONT.

4.2. Tephra

Scoria lapilli FS and ET0901 are both almost aphyric (phenocrysts <5 and <10 vol.%, respectively). The phenocryst assemblage consists of euhedral to subhedral olivine (up to 1 mm in length) followed by subhedral clinopyroxene (0.5–2 mm in length). Plagioclase is absent in FS tephra, while plagioclase microphenocrysts occur in small amounts in ET0901 scoria.

The groundmass of the FS sample is glassy with very rare microlites of clinopyroxene and olivine, whereas that of ET0901 is glassy with portions exhibiting variable enrichment in micro-opaques.

Olivine phenocrysts of FS are Fo_{90-92} whereas the Mg content varies in ET0901 samples (Fo_{72-89}). The clinopyroxene composition is $Wo_{42-43}En_{44-47}Fs_{4-6}$ for FS and $Wo_{44-46}En_{32-35}Fs_{6-11}$ for ET0901. Plagioclases in ET0901 are An_{51-66}.

The Mg-rich olivine in the FS scoria lapilli and the picritic whole-rock composition represent the most-primitive compositions of the overall Etnean magmatism and allow the FS to be defined as a primary magma that has not suffered significant modification after extraction from its mantle source (Coltelli et al., 2005).

The MAL sample, although also primitive, has a more-variable olivine composition than FS, and also some peculiar trace-element and isotopic patterns (Armienti et al., 1988; Corsaro and Pompilio, 2004) that require more complex source processes in addition to some stages of crystallization (see discussion in Kamenetsky and Clocchiatti, 1996); this argument can be partially extended to SPA.

5. Results

5.1. Major and trace elements

Major-element compositions of our samples (Table 1, Fig. 2) have already been widely investigated, and our results are consistent with those of previous studies (red symbols in Fig. 2; data from Armienti et al., 1988, 2004; Clocchiatti et al., 2004; Coltelli et al., 2005; Corsaro et al., 2006, 2009; Tanguy et al., 1997; Viccaro and Cristofolini, 2008; Viccaro et al., 2006). The samples include picritic basalts (sample FS), basalts (MAL and MONT), trachybasalts (DEF and SPA) and a tephrite–basanite (ET0901).

Fig. 2 compares our data with those of the main historical eruptions of Mt. Etna. In particular, we discern the fields of the tholeiitic lavas (i.e., the oldest of Mt. Etna; data from Armienti et al., 2004; Tanguy et al., 1997) from all of the other alkaline lavas, distinguished in pre- and post-1971 (Armienti et al., 1994; D'Orazio et al., 1997; Finocchiaro, 1995; Joron and Treuil, 1984). Lavas erupted after 1971 are characterized by a higher K content (Armienti et al., 1994; Clocchiatti et al., 1988, 2004; Corsaro and Pompilio, 2004; Métrich et al., 2004; Viccaro and Cristofolini, 2008). Our sample compositions confirmed the temporal trend: lavas and tephra erupted between 15 ky and ~400 y BP (i.e., MAL, SPA, MONT, ET0901 and FS) correspond to the most-primitive composition of pre-1971 volcanic rocks, and the 1974 lava (DEF) falls within the trachybasaltic field, where the post-1971 magmas appear on the plot.

The investigated rocks are among the most-primitive lavas that have been erupted at Mt. Etna, showing the lowest Na_2O, K_2O and SiO_2 contents (Fig. 2). This primitive nature is also highlighted in the plot of MgO versus CaO/Al_2O_3 in Fig. 3. Comparing alkaline and tholeiitic lavas in this figure reveals that the studied lava/tephra represent some of the least evolved alkaline products of the Etnean history, with FS being the most-primitive magma.

Fig. 4 shows that all studied samples exhibit a similar LREE enrichment (La_n/Yb_n = 11–26) comparable to that found in other Etnean products (tholeiites and pre- and post-1971 alkaline lavas; data from Armienti et al., 2004; Corsaro and Pompilio, 2004; Cristofolini et al., 1991; D'Orazio et al., 1997; Viccaro and Cristofolini, 2008). A difference in REE concentrations between the investigated samples is also evident, increasing from FS picrite to ET0901 and SPA (Fig. 4). For comparison with a potential reference mantle source, we report also the REE pattern of Hyblean peridotites (data from Correale et al., 2012; Sapienza and Scribano, 2000). The patterns are comparable, although our products are richer in REE relative to Hyblean xenoliths.

The MORB-normalized multi-element diagram (Fig. 5) displays a humped pattern common to all studied samples, and due to different degrees of enrichment between the LILE (e.g., K, Ba and Rb) and HFS elements (e.g., Zr, Nb and Hf). Both LILE and HFS elements of each sample are enriched (to varying degrees) relative to MORB. Comparison of these results with those from OIB- and arc-type volcanism suggests a composition intermediate between the two types.

Fig. 6 shows the plots of the ratios of highly incompatible trace elements, that are little affected by later crystal fractionation processes and so reflect source characteristics (see also Fig. 11). We selected incompatible elements that are fluid-immobile (except La) and whose concentration in the melt is controlled only by source chemistry and crystal/melt processes during melt genesis and evolution. Our results are consistent with the literature data (red symbols in Fig. 6; data from Armienti et al., 2004; Coltelli et al., 2005; Corsaro et al., 2009; Viccaro and Cristofolini, 2008) for products from the same eruptions, confirming a homogeneous composition. The investigated products are compared to literature data for tholeiitic, pre- and post-1971 alkaline lavas (Armienti et al., 2004; Corsaro and Pompilio, 2004; Cristofolini et al., 1991; D'Orazio et al., 1997; Viccaro and Cristofolini, 2008) and also mantle xenoliths (peridotites and pyroxenites; Correale et al., 2012; Sapienza and Scribano, 2000) from the Hyblean Plateau. All of our samples plot partially within the field of post-1971 alkaline lavas, with FS approaching the field for tholeiites. Compared to Hyblean mantle xenoliths, the rocks in this study plot overlap with the composition of peridotites, suggesting a close similarity of their mantle sources with the Hyblean mantle. In Fig. 6, Etnean products are characterized by trends whose end-members are always represented by SPA and FS lavas.

5.2. Sr–Nd isotopes

Sr and Nd isotopic analyses of the studied samples are listed in Table 1 and plotted in Fig. 7. The $^{143}Nd/^{144}Nd$ ratio is highest for

Table 1
Major elements, trace elements and Sr–Nd isotopic ratios for whole-rock studied samples.

	DEF	MAL	MONT	SPA	FS	ET0901
SiO_2 (wt.%)	46.20	47.47	46.93	48.46	45.05	44.57
TiO_2	1.76	1.51	1.61	1.52	0.83	1.63
Al_2O_3	16.34	14.71	16.59	15.15	9.32	16.10
$Fe_2O_{3\ TOT}$	11.64	11.87	11.39	10.36	10.25	11.70
MnO	0.19	0.19	0.18	0.17	0.16	0.17
MgO	6.33	8.05	6.27	7.68	17.58	7.03
CaO	11.35	12.33	10.91	11.58	11.02	8.86
Na_2O	3.36	2.52	3.38	3.75	1.12	2.78
K_2O	1.91	1.18	1.34	1.39	0.51	0.89
P_2O_5	0.53	0.44	0.49	0.65	0.21	0.63
LOI	0.8	1.2	0.8	0.9	–	–
Total	99.5	101.5	99.9	101.5	96.0	94.4
Mg#	51.9	57.3	52.2	59.5	77.3	54.3
La	62.5	49.4	53.6	81.0	27.9	87.3
Ce	116	95.0	101	151	62.5	171.2
Pr	13.6	11.3	11.8	17.4	6.7	17.4
Nd	53.5	45.4	46.3	66.9	27.6	65.6
Sm	10.2	8.8	8.7	11.7	5.6	11.4
Eu	3.07	2.57	2.58	3.35	1.61	3.12
Gd	9.69	8.51	8.18	10.7	5.58	10.7
Tb	1.23	1.09	1.03	1.24	0.75	1.27
Dy	5.72	5.22	4.74	5.59	3.57	5.53
Ho	1.10	1.02	0.93	1.07	0.75	1.11
Er	3.00	2.84	2.55	2.89	2.09	3.12
Tm	0.38	0.36	0.32	0.36	0.27	0.39
Yb	2.45	2.33	2.08	2.28	1.78	2.56
Lu	0.33	0.33	0.29	0.32	0.24	0.36
Sr	1412	1048	1149	1573	396	934
Rb	50.6	30.0	23.7	33.5	11.0	16.1
Ba	717	580	591	817	255	755
U	2.27	2.04	1.98	3.20	1.05	3.76
Th	8.15	7.52	6.06	11.9	3.38	13.0
Ta	2.87	2.01	2.62	3.97	0.92	3.60
Nb	57.8	39.6	53.5	82.0	17.5	78.6
Zr	244	166	197	250	87	221
Hf	5.17	4.01	4.60	5.36	2.20	5.07
Y	29.1	27.3	23.5	28.1	20.0	30.3
$^{87}Sr/^{86}Sr$	0.703574 ± 6	0.703687 ± 6	0.703410 ± 6	0.703317 ± 6	0.703910 ± 6	0.703361 ± 6
	0.703577 ± 6	0.703707 ± 6	0.703420 ± 6	0.703325 ± 6		
$^{143}Nd/^{144}Nd$	0.512865 ± 4	0.512873 ± 4	0.512909 ± 4	0.512908 ± 5	0.512836 ± 6	0.512913 ± 6

Mg# = 100 × Mg/(Mg + Fe_{tot}); LOI = loss on ignition.

ET0901, MONT and SPA and lowest for MAL, DEF and FS. The average $^{87}Sr/^{86}Sr$ ratios vary from the most primitive values for SPA of 0.7033 to the more evolved value for FS of 0.7039. For comparison we report average Sr–Nd isotopic data for products from the same eruptions (red symbols in Fig. 7; data from Armienti et al., 2004; Kamenetsky and Clocchiatti, 1996; Viccaro and Cristofolini, 2008). The samples of this study and those in the literature are generally similar, with ET0901, MONT and SPA showing the most-depleted compositions among the investigated samples (i.e., least radiogenic Sr and most radiogenic Nd). Fig. 7 also plots the isotopic compositional fields of other products from Mt. Etna (Armienti et al., 2004; Tonarini et al., 2001; Viccaro and Cristofolini, 2008). The Sr–Nd isotopic values of these rocks show an inverse correlation between Sr and Nd, where tholeiitic lavas have the highest $^{143}Nd/^{144}Nd$ and lowest $^{87}Sr/^{86}Sr$ (typical of uncontaminated depleted mantle), while recent alkaline lavas have the lowest $^{143}Nd/^{144}Nd$ and highest $^{87}Sr/^{86}Sr$ (typical of mantle affected by contributions of enriched materials). Our samples plot (according to their ages) in the fields of Etnean pre- and post-1971 alkaline lavas, and are located in a zone corresponding to products with an intermediate-to-high degree of crustal contamination.

Fig. 7 also shows the isotopic data of Hyblean mantle peridotite and pyroxenite xenoliths (Bianchini et al., 2010; Correale et al., 2012; Tonarini et al., 1996). All investigated products fall in the range of $^{143}Nd/^{144}Nd$ values of Hyblean mantle, but have higher $^{87}Sr/^{86}Sr$ ratios.

5.3. He isotopes

Investigations of noble-gases characteristics (abundances of He, Ne and Ar, and He–Ar isotopic ratios) of fluid inclusions hosted in olivine and pyroxene phenocrysts from Mt. Etna are reported here. The low $^4He/^{20}Ne$ and $^{40}Ar/^{36}Ar$ ratios (mean values of 29 and 319, respectively) indicate the presence of an atmospheric component, consistent with previous studies (Marty et al., 1994; Nuccio et al., 2008). Owing to the low He content in air, $^3He/^4He$ values are almost unaffected by the atmospheric contribution (Table 2).

The $^3He/^4He$ ratio, reported as Rc/Ra value (with Ra from the $^3He/^4He$ ratio in atmosphere of 1.39×10^{-6}), is relative to the He isotopic ratio corrected for air contamination (Giggenbach et al., 1993) and ranges from 6.69 Ra for MONT to 7.62 Ra for SPA olivines, and from 4.87 for DEF to 6.59 for SPA pyroxenes (Table 2, Fig. 8). Fig. 8 compares the $^3He/^4He$ ratio and He concentration of our samples with other products of Mt. Etna (Marty et al., 1994; Nuccio et al., 2008). Our data set is consistent with these studies and confirms that olivines are richer in He and display higher Rc/Ra ratios than pyroxenes. Disequilibrium between isotopic values of cogenetic olivine and pyroxene hosted fluid inclusions is a widely debated issue for lavas from Mt. Etna (Coulson et al., 2011; Marty et al., 1994; Nuccio et al., 2008) and other basaltic volcanoes (Hilton et al., 1995; Shaw et al., 2006). However, there is agreement that mantle signatures are preserved more faithfully by olivine phenocrysts than by pyroxenes (Hilton et al., 2002; Marty

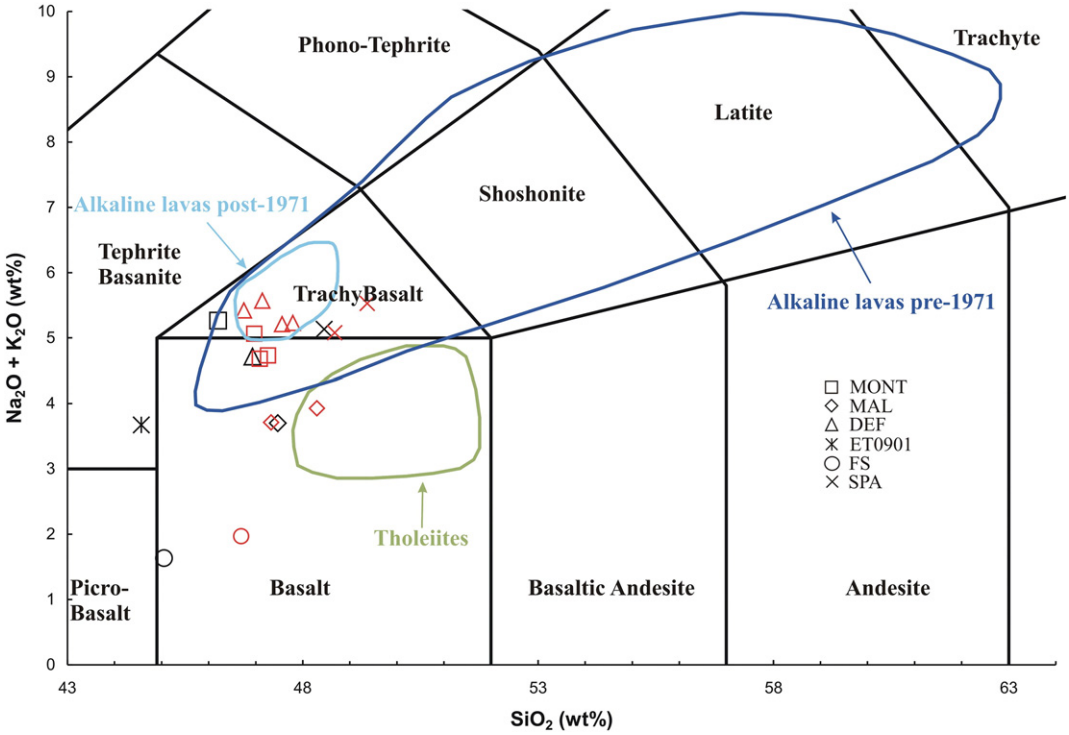

Fig. 2. Total alkali-silica classification diagram (Le Maitre, 2002) for studied samples. The red symbols indicate data from literature analyses of investigated mafic and/or eccentric eruptions of Mt. Etna. Colored fields correspond to (i) ancient Etnean tholeiites (green contour), (ii) pre-1971 alkaline lavas (dark-blue contour) and (iii) post-1971 alkaline lavas (light-blue contour). Literature data reference in the text.

et al., 1994; Nuccio et al., 2008; Shaw et al., 2006). We therefore focus our discussion on results for olivine. Fig. 8 also compares data from Etnean olivines and clinopyroxenes with those from Hyblean peridotites and pyroxenites (Correale et al., 2012; Sapienza et al., 2005). Only the most primitive values for olivines of SPA and MAL are compatible with the Hyblean mantle; the remaining samples (FS, MONT and DEF) display He isotope ratios lower than those for Hyblean mantle.

$^3He/^4He$ values for olivine phenocrysts of the investigated products relative to their estimated ages are shown in Fig. 9. Lavas, which erupted <3930 y BP (DEF, MONT, ET0901 and FS), show average $^3He/^4He$ values (~6.8 Ra) that are slightly lower than those of the oldest rocks (MAL, SPA) with ages between 4 and 15 ky BP that have $^3He/^4He$ ratios of 7.1–7.6 Ra. For comparison, we also report the $^3He/^4He$ value measured in the ancient Etnean tholeiites (Marty et al., 1994) and in the two DDF eruptions of 2001 and 2002–2003 ($^3He/^4He$ values of ~6.9 Ra; Nuccio et al., 2008). We also report gas emissions sampled during the 2001 eruption (Caracausi et al., 2003); for these the $^3He/^4He$ ratio peaks at 7.6 Ra and coincides with the highest $^3He/^4He$ measured in fluid inclusions of SPA.

6. Discussion

6.1. Modeling of source partial melting and crystal fractionation processes

Differences in the REE concentrations of the investigated samples (Fig. 4) are attributable to a decreasing degree of partial melting of a

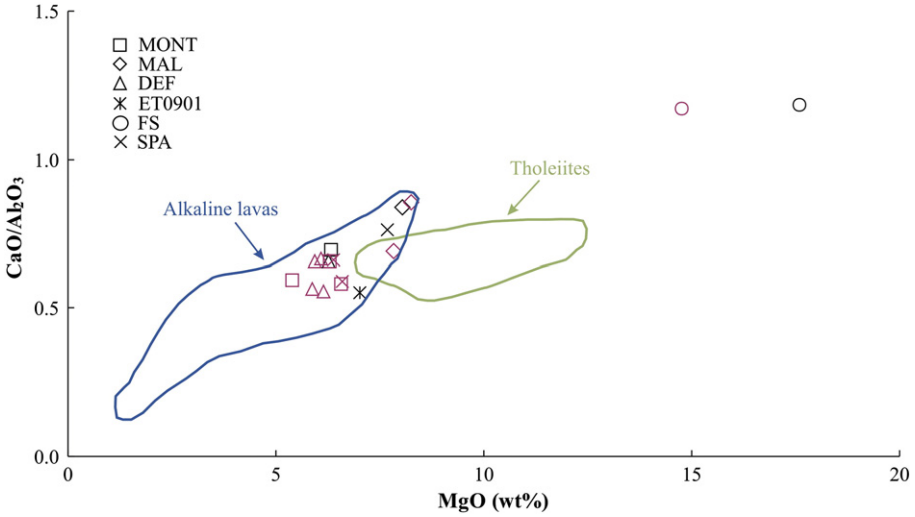

Fig. 3. CaO/Al_2O_3 ratio versus MgO for whole-rock studied samples. The colored fields indicate ancient Etnean tholeiites (green contour) and historical to recent alkaline lavas (blue contour). Literature data as in Fig. 2.

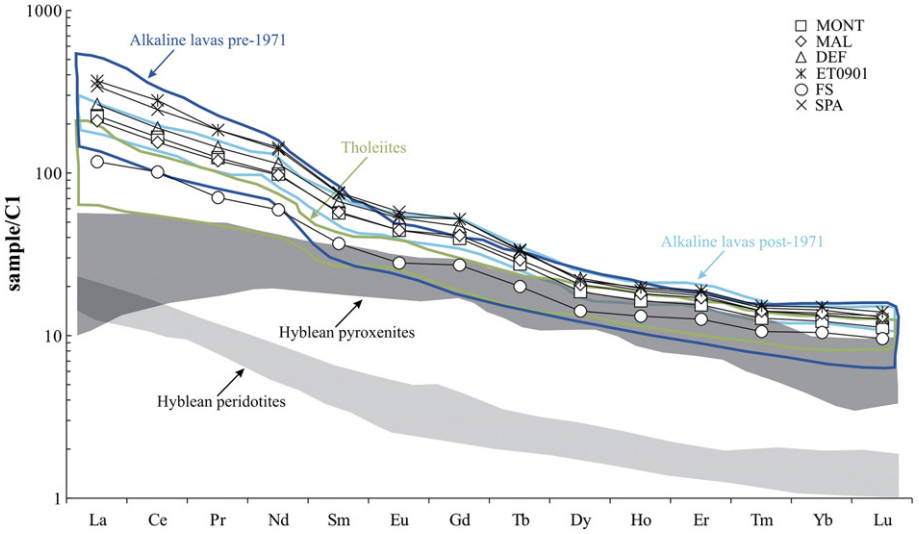

Fig. 4. REE patterns for whole-rock studied samples. The colored fields (green, dark blue and light blue) correspond to tholeiites and to pre-1971 and post-1971 alkaline lavas, respectively. The light- and dark-gray shaded areas correspond to the REE patterns of Hyblean peridotites and pyroxenites, respectively. Normalization to C1 chondrite is after Sun and McDonough (1989). Literature data reference in the text.

common mantle source, an increasing degree of crystallization, or both of these processes. In this section we present models of both partial melting of the mantle source and low-pressure equilibrium crystallization, and compare the modeling results with those obtained from the studied samples. We assumed a starting mantle composition of a lherzolite xenolith from the Hyblean Plateau (Correale et al., 2012). Our approach is outlined below.

Firstly, in order to simulate partial melting, we started from the major-element compositions of XIH-3 Hyblean lherzolite (olivine = 50%, orthopyroxene = 11%, clinopyroxene = 8%, spinel = 3%, serpentine = 18% and carbonate = 10%; Correale et al., 2012). Using the MELTS program (Ghiorso and Sack, 1995) to model the batch melting process, we computed the major element compositions of melts generated by increasing the melting percentages. Thermobaric constraints for the modeling were a pressure of ~1 GPa and a temperature of about 1260 °C. This pressure is compatible with the reported pressure at the depth from which Etnean magma originates (1–3 GPa; Armienti et al., 1988, 2007; Corsaro and Pompilio, 2004) and with microthermometric determinations of fluid inclusions in Hyblean xenoliths (about 1 GPa; Sapienza et al., 2005), while the selected temperature is in accordance with the quenching temperature of Etnean melt inclusions (up to 1240 °C; Kamenetsky and Clocchiatti, 1996) and segregation temperatures (up to 1230 °C for alkali basalts) estimated for Hyblean melts by Beccaluva et al. (1998). Redox conditions were set at fO_2 = QFM in accordance with Perinelli et al. (2008) for the local upper mantle. We simulated three different conditions of partial melting, namely isobaric, isothermal and flux melting of the lherzolite. In isobaric conditions (1 GPa), solidus conditions were achieved by increasing the temperature to 1310 °C, whereas a temperature of 1390 °C was required to achieve 10% of melting. These temperatures are higher than the values given above, making isobaric melting unlikely. In isothermal mode the temperature was set to 1260 °C, and the pressures (0.3–0.7 GPa) necessary to reproduce the major element compositions of studied products would involve melting in the crust. This process would also give unrealistic results, and so can be excluded. Finally, flux melting was simulated by adding H_2O to the source at 1260 °C and 1 GPa. Our calculations show that increasing the H_2O content from 0.01 to 0.3 wt.% produces melting up to 10%, thereby satisfying all of the given constraints. Fig. 10 reports the variations in the compositions of some major elements (Mg, Na, Al and Ca) as a result of flux melting.

Secondly, starting from the computed melt composition achieved by flux melting, we simulated the equilibrium crystallization of these

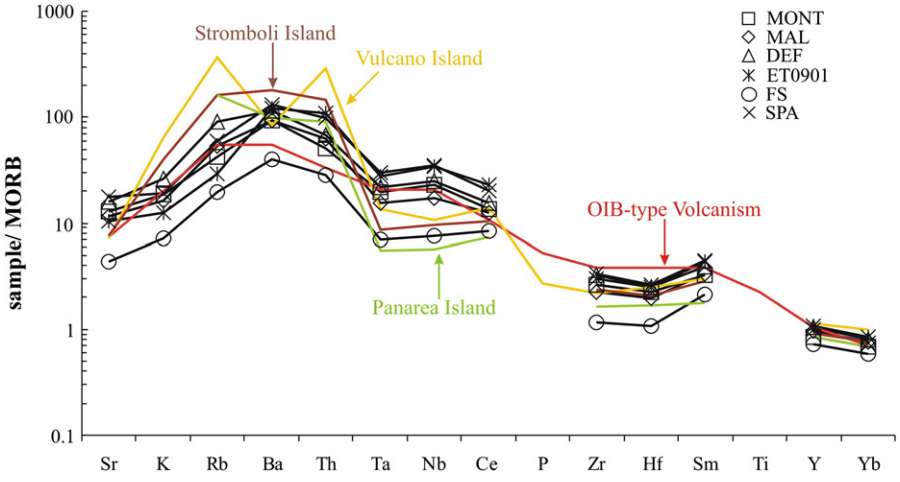

Fig. 5. Diagram for whole-rock studied samples. Data of OIB-type volcanism are from Sun and McDonough (1989), while data of arc-type volcanism (Vulcano, Stromboli and Panarea Islands) are average values from compilation data of Peccerillo (2005). Normalization to MORB is in accordance with Sun and McDonough (1989).

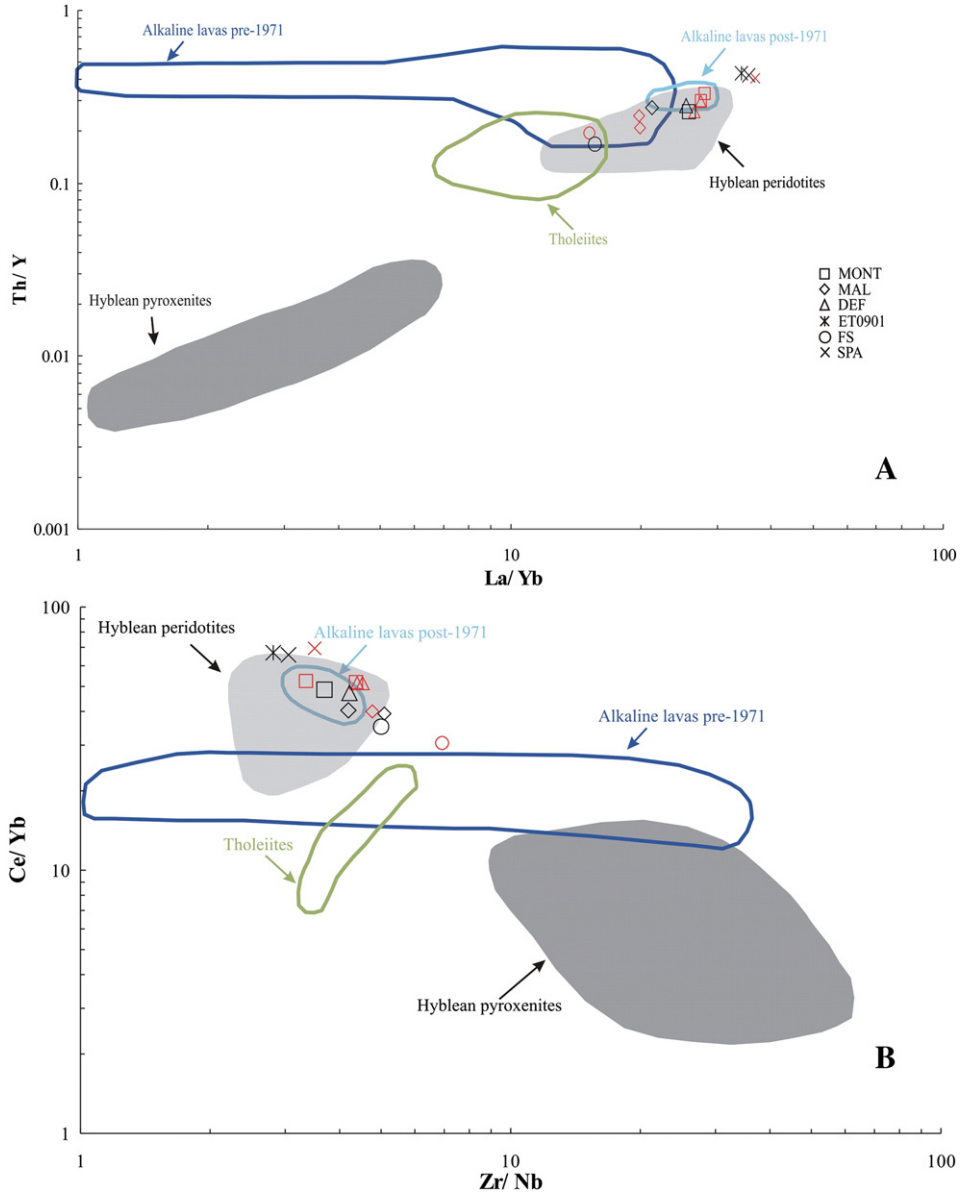

Fig. 6. Plots of Th/Y versus La/Yb (A) and Ce/Yb versus Zr/Nb (A) for whole-rock studied samples. Red symbols are literature data of products from the same studied eruptions. Colored fields are as in Fig. 2. The shaded gray areas are as in Fig. 4. Literature data reference in the text.

melts. The proposed crystallization trajectories represent only some of all those possible for a melt at Mt. Etna (see also Corsaro and Pompilio, 2004, for detailed results). We considered isobaric crystallization at 0.4 GPa induced by decreasing the temperature from ~1260 °C to 1050 °C, with a variable H_2O content depending on the starting melt and fO_2 = NNO + 1. The redox conditions are those defined by Liotta et al. (2012), while the chosen pressure was similar to that estimated by Corsaro and Pompilio (2004) for the deep Etnean magma reservoir where magma is normally stored, cools and evolves. This pressure is also consistent with the range of depths inferred from geophysical studies (De Gori et al., 2005; Mattia et al., 2007) and with that estimated using the He/CO_2, He/Ne and He/Ar ratios measured in Etnean gas emissions (Paonita et al., 2012). Fig. 10 presents the modeled crystallization paths for the selected major elements (Mg, Na, Al and Ca). Comparison of the computed curves with the compositions of Etnean lavas/tephra shows that a variable degree of partial melting of the model mantle source, followed by equilibrium crystallization, is able to fully represent the entire compositional range exhibited by the studied products. The modeling results can be interpreted as indicating that the studied samples derive from low to high degrees of partial melting, increasing from ~1% at SPA, through ~2% at DEF and MONT, ~3% at MAL and ET0901, and up to ~10% at FS, with the degrees of crystallization of olivine and clinopyroxene being similar for all of the samples, ranging from 6% to 10%. FS is the only sample showing negligible crystallization.

It should be noted that we carried out melting plus crystallization simulations using less altered lherzolite than the XIH-3 sample (i.e., LOI = 1.8 and 0.8 for samples HYB 29 and 36, respectively; Perinelli et al., 2008). These changes in composition affected the major-element contents of the obtained melts and so reduce the melting range (from 1.5–2% for SPA to 7% for FS) and increase the degree of crystallization (up to about 20%) estimated for the investigated Etnean products. Finally, since the MELTS program can also be used to calculate the mineral composition at any crystallization stage, the model phenocrysts were compared with the compositions of olivine and pyroxene in the studied rocks. This revealed a reasonably good match between the model and natural phenocryst compositions (see Supplementary Tables A1 and A2).

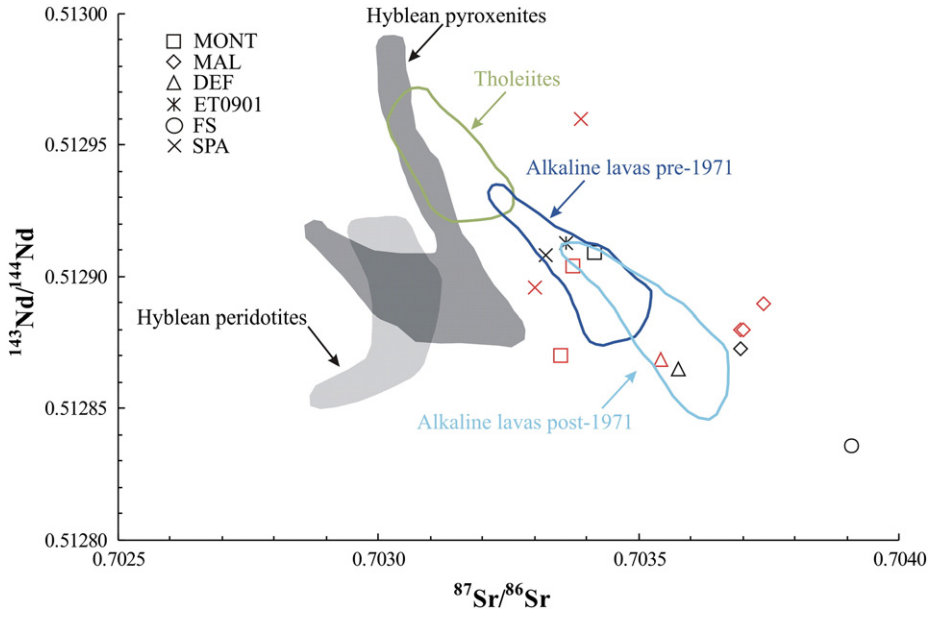

Fig. 7. Sr–Nd isotopic compositions of whole-rock studied samples. Red symbols are literature data of products from the same studied eruptions. The colored fields are as in Fig. 2. The shaded gray areas are as in Fig. 4. Literature data reference in the text.

Thirdly, once we obtained the fractions of batch melting and crystallization, we calculated the initial trace element compositions of the mantle source from their contents measured in each sample. We used the equation for modal batch melting to determine a possible mantle source composition for selected incompatible trace elements (Zr, Nb, Ce, Yb, Th, La, Y and Ta); the results are represented in Fig. 6:

$$C_i^s = C_i^l \times [D(1-F) + F] \quad [1]$$

where C^l_i and C^s_i are the concentrations of the *i*-th element in the melt and solid source, respectively; *F* is the melting fraction, which varies from 0 to 1; and *D* is the bulk partition coefficient of the given element (corresponding to the weighted mean of the mineral content in the mantle assemblage) (Wilson, 1989). The mineral–melt partition coefficients were taken from those specific for mafic and ultramafic melts (White, 2007).

The calculated trace element concentrations of the modeled mantle sources are reported in Fig. 11, in which it is evident that partial melting is the principal process able to generate substantial variations in trace-element ratios, while crystal fractionation even as high as 20% produces only minor changes. Fig. 11 also shows that the calculated trace element ratios (Zr/Nb versus Ce/Yb and Th/Y versus La/Yb) of the modeled mantle sources fall into a rather small area. In order to obtain a more robust data set, we extended the simulations (i) to tholeiitic products from the ancient activity of Mt. Etna (Armienti et al., 2004; Corsaro and Cristofolini, 1997) and (ii) to lavas of the 2001 eruption. The 2001 eruption was characterized by the synchronous eruption of two magma types with different petrographic and geochemical features (Clocchiatti et al., 2004; Métrich et al., 2004), and we chose the most primitive, which erupted from an eccentric vent. The unrealistically low degree of source partial melting (around 1%; not shown in the figure) found for ancient tholeiitic lavas suggests that these products originated from a mantle source

Table 2
Chemical and isotopic compositions of noble gases from fluid inclusions entrapped in olivine and pyroxene phenocrysts.

Sample	Mineral	^{4}He 10^{-13} (mol/g)	^{20}Ne 10^{-15} (mol/g)	^{40}Ar 10^{-13} (mol/g)	R/Ra	Rc/Ra	Error +/−	^{40}Ar/^{36}Ar	Error +/−
DEF	Cpx	9.9	1.4	6.1	6.73	6.73	0.06	328.6	0.88
		5.9	2.6	4.0	6.70	6.71	0.13	308.5	0.31
	Oliv	1.2	3.0	18.5	5.54	5.58	0.16	304.2	0.05
		0.4	2.3	–	4.79	4.87	0.64	–	–
MAI	Oliv	5.2	0.6	4.4	7.13	7.13	0.13	321.4	0.32
		5.8	1.5	2.6	7.14	7.15	0.16	339.0	0.34
MONT	Cpx	7.1	2.0	2.3	6.68	6.69	0.10	331.7	0.06
		8.0	1.8	4.0	6.82	6.82	0.14	335.8	0.97
	Oliv	0.7	4.2	13.6	5.11	5.19	0.20	303.0	0.05
		0.8	2.7	19.1	5.78	5.84	0.39	298.8	0.15
SPA	Cpx	21.8	2.3	8.1	7.62	7.62	0.10	417.9	0.42
		14.9	2.2	8.8	7.57	7.57	0.09	354.0	0.35
	Oliv	1.2	3.9	8.0	6.53	6.59	0.45	308.9	0.31
		0.5	3.3	5.4	4.42	4.50	0.28	296.0	0.30
FS	Cpx	5.4	2.6	5.0	6.70	6.71	0.13	319.1	0.93
		3.0	12.4	108.1	6.76	6.84	0.17	296.1	0.30
	Oliv	3.0	4.0	16.5	6.23	6.25	0.16	295.8	0.86
		2.5	4.5	5.8	6.39	6.43	0.16	302.3	0.30
ET0901	Cpx	5.9	27.1	88.0	6.72	6.81	0.14	–	–
		9.3	1.2	1.9	7.21	7.21	0.14	308.0	0.31
	Oliv	2.4	7.9	1.4	6.48	6.55	0.13	309.7	0.05
		1.9	1.3	2.5	6.36	6.37	0.19	300.6	0.30

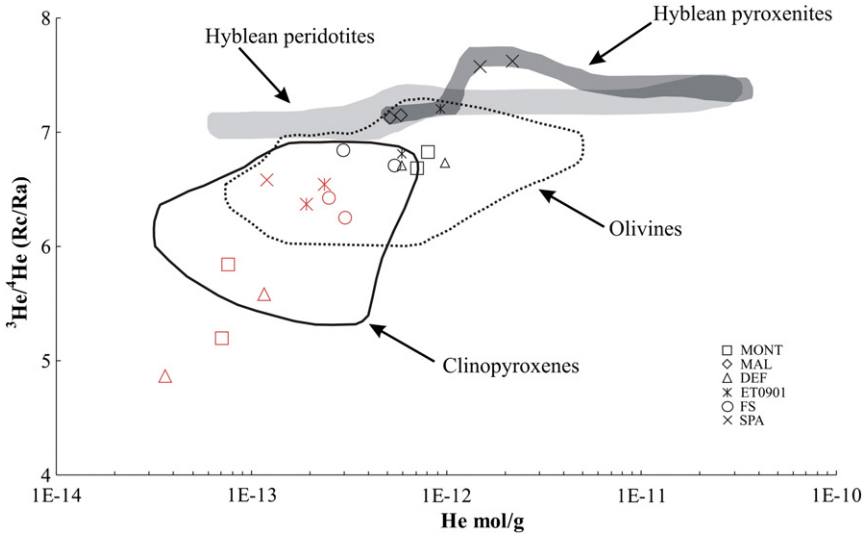

Fig. 8. Plot of $^3He/^4He$ (in Rc/Ra) versus He abundance from fluid inclusions hosted in olivines and pyroxenes separated from the investigated Etnean products. The Rc/Ra values are corrected for air contamination (see Giggenbach et al., 1993). Gray and red symbols are for the olivines and pyroxenes, respectively. The dashed and continuous circles define the compositional ranges of previous investigations carried out on olivines and clinopyroxenes from other Etnean eruptions. The shaded gray areas are as in Fig. 4. Literature data reference in the text.

different from the one we used to model the petrogenesis of alkaline lavas. In contrast, the results from the 2001 eruption provide evidence that the geochemical marker of the mantle source that fed the 2001 eruption is similar to those of the eruptions during the past 15 ky. A similar conclusion supporting a common mantle source for Etnean products was suggested by Coulson et al. (2011) based on a geochemical investigation of some eccentric Etnean products.

It is noteworthy that the trace element composition of the modeled Etnean mantle source is not affected by large variations if we apply the melting and crystallization percentages estimated for the lherzolites altered less than the XIH-3 sample. Therefore, the degree of alteration of the starting lherzolite does not seem to influence the conclusions that can be drawn from our model.

Finally, we compare the results obtained by hypothesizing a two-layer mantle for the source of Hyblean magmatism (Correale et al., 2012). Fig. 11 clearly reveals that the Etnean source plots along a mixing curve that joins the two end-members (i.e., peridotitic and pyroxenitic Hyblean mantle sources). The recalculated Etnean mantle source was mainly peridotitic nature in terms of its trace-element signature, however, a significant contribution (~10%) from pyroxenites can also be recognized.

6.2. Sr and Nd isotopes

Several hypotheses have been formulated to explain the Sr and Nd isotope variations of Etnean lavas. Armienti et al. (2004), Tonarini et al. (2001) and Viccaro and Cristofolini (2008) proposed the presence of crustal fluids derived from dehydration of the subducting Ionian slab. An alternative process of crustal contamination by fluids was hypothesized by Michaud (1995), who proposed isotope exchanges between

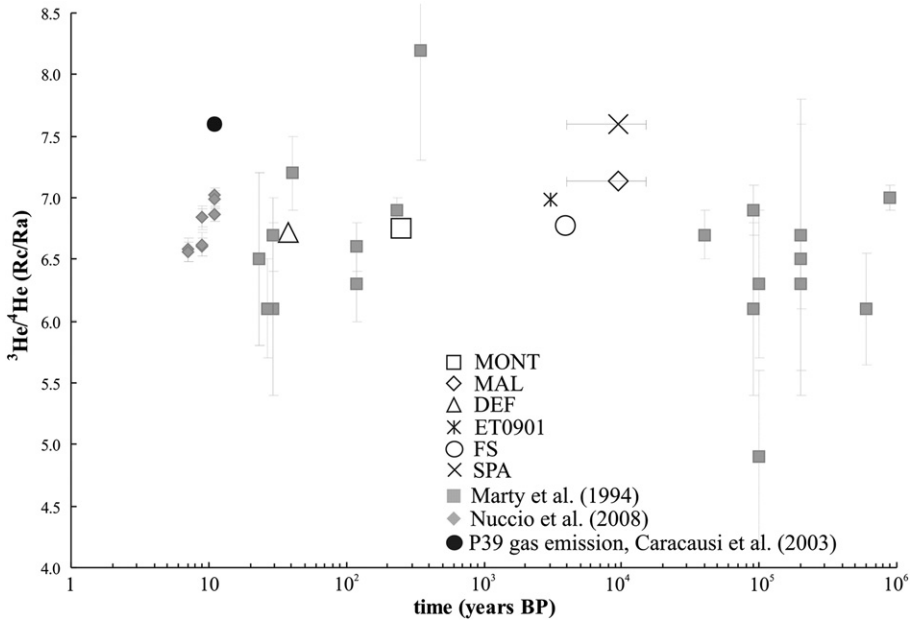

Fig. 9. Plot of $^3He/^4He$ (in Rc/Ra) from olivine phenocrysts versus time for the studied samples. The ages of the prehistorical Etnean products are from Branca et al. (2011b), Coltelli et al. (2005) and Del Carlo et al. (2004). The age uncertainty of SPA and MAL samples (Branca et al., 2011b) is represented by a horizontal error bar. Error bars in our data set lie within the symbol size.

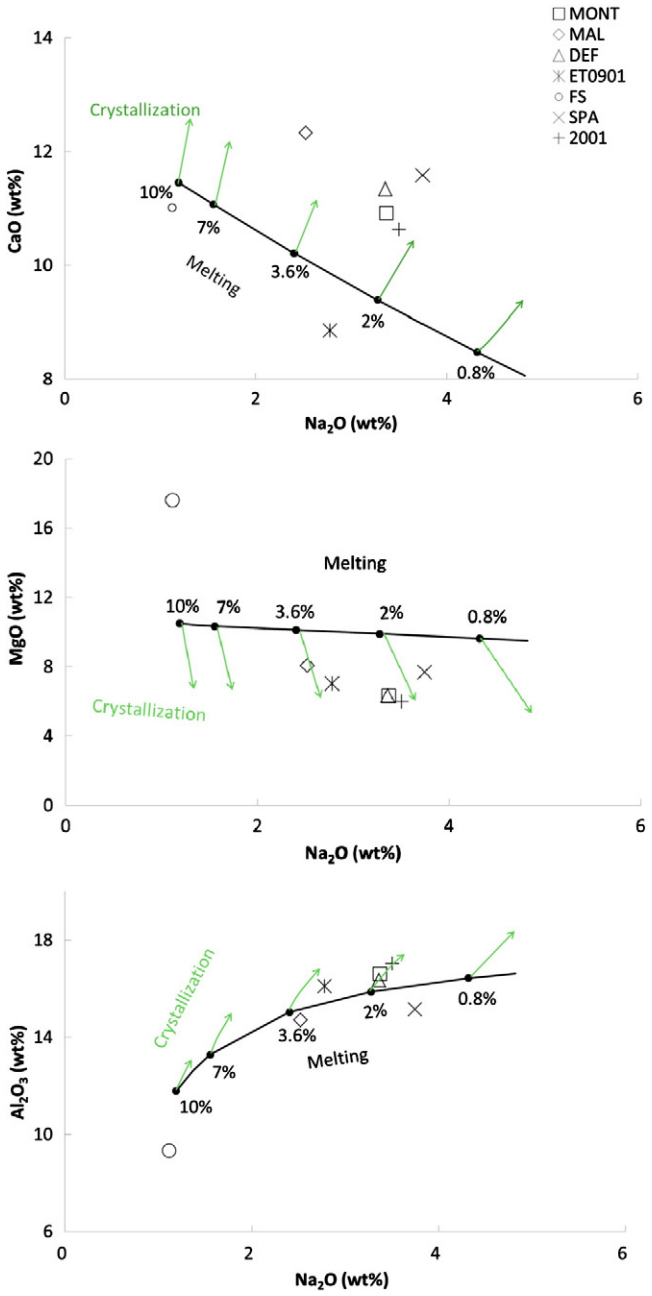

Fig. 10. Variations in major-element melt composition induced by variable degrees of flux melting (black curve) and equilibrium crystallization (EC; green arrows). The lengths the green arrows correspond to about 10% of crystallization. Numbers on the partial melting curve indicate weight percentages of melting.

magma and sedimentary rocks of the basement of the volcano. Armienti et al. (2004) also suggested that the main trend of Sr and Nd isotopes of Etnean products, attributed to crustal contamination by fluids, is coupled to a second-order variability characterized by a steeper slope than the former and attributed to <3% crustal contamination. Shallow-level contamination has also been hypothesized for MAL magma (Armienti et al., 2004; Tonarini et al., 2001). Model calculations by Tonarini et al. (2001) showed that the measured data for B and Sr isotopes can be obtained when Etnean magmas assimilate less than 10% of a sedimentary component. Based on these interpretations, variable magma contamination by crustal materials can account for the enriched values in our data set, regardless of whether it occurred close to the surface or as recycling in the mantle. In detail, the more-primitive isotope values of SPA, ET0901 and MONT reflect both peridotitic and pyroxenitic contributions, but only according to the Nd isotope data (Fig. 7). Focusing our attention on the LILE enrichment (see Section 5.1), we propose that fluids of crustal origin could have shifted the isotope marker of magmas towards more-enriched values of DEF, MAL and finally FS. Section 6.5 discusses how this contribution affects our modeling of the mantle source.

6.3. Noble gases from fluid inclusions

The highest value of $^3He/^4He$ sampled at Mt. Etna from gas emissions by Caracausi et al. (2003) (see Section 5.3) during the 2001 eruption (Fig. 9) was attributed by those authors to the isotope marker of the volatile-rich magma recharging the shallow plumbing system, and it has been suggested that $^3He/^4He$ is 7.6 Ra for the present-day mantle feeding Etnean magmatism. This is the same as our value for SPA olivine. It is unlikely that the SPA value is influenced by a post-eruptive accumulation of cosmogenic ^3He, because this sample has the highest He elemental concentration among those investigated and is, therefore, the least prone to isotope variation due to post-eruptive He accumulation. Furthermore, the single-step crushing procedure is known to minimize radiogenic–cosmogenic components (e.g., Burnard et al., 1999; Marty et al., 1994). No contribution of cosmogenic He was reported by Marty et al. (1994) even in samples as old as 500 ky. The high value for SPA is therefore a characteristic of the Etnean mantle source, which means that the $^3He/^4He$ value of Etnean mantle source has been at least 7.6 Ra since at least 15 ky BP.

$^3He/^4He$ values lower than 7.6 Ra measured in both historical (DEF and MONT) and prehistorical (FS, ET0901 and MAL) samples are probably not indicative of the mantle source, being influenced by secondary processes that occurred before or after the eruption. It is highly unlikely that the decrease in $^3He/^4He$ is due to the post-eruptive radiogenic production of ^4He, because similar isotope values (~6.6 Ra) are common in Etnean olivines from present-day activity (Nuccio et al., 2008) where post-eruptive ^4He accumulation is negligible. Also, three samples (DEF, MONT and MAL) that have different ages and comparable U and Th contents show a subhorizontal or slightly positive trend in a plot of $^3He/^4He$ versus time (Fig. 9), in contrast to what is expected for radiogenic accumulation. Therefore, $^3He/^4He$ values of ~6.6 Ra are due to the pre-eruptive addition of ^4He resulting from magma aging and/or crustal contamination of magma.

Although Nuccio et al. (2008) rejected these two processes when attempting to justify the decrease in R/Ra observed in products from the 2001 to the 2004 eruption, these processes could act over longer time periods. In terms of magma aging, radiogenic ^4He accumulation from U and Th measured for example in MONT and DEF lavas is $\sim 2.5 \times 10^{-13}$ mol/g over 10 ky, a timescale that is the maximum estimated for magma chamber refilling at Mt. Etna (Condomines et al., 1982, 1987). Calculating the effect of this ^4He accumulation on a lowering of the magmatic R/Ra requires knowledge of the pristine (unradiogenic) He content per gram of melt. This value cannot be strictly related to the He content in fluid inclusions of olivines (which is the quantity that we measured), because this can vary with the number of entrapped vesicles. If the He concentration in the fluid inclusions retained in a melt from Mt. Etna is similar to that of the olivines, the calculated radiogenic accumulation would decrease the $^3He/^4He$ values of MONT and DEF olivines by ~2 Ra units. This estimate constitutes an upper limit to the effect of ^4He accumulation, so the extent of the magma aging might be broadly consistent with the observed shift from the "pure" magmatic value (7.6 Ra) to lower values (e.g., 6.6 Ra, as commonly seen in Etnean olivines from present-day activity).

Crustal contamination is also difficult to constrain quantitatively. Based on the diffusivity of He in melts (5×10^{-5} cm^2/s; Lux, 1987), a long timescale of 10 ky can account for the diffusion of radiogenic ^4He towards the magma body by several tenths of meters. The advective dynamics of magma could subsequently contribute to mixing of the entire reservoir. Thus, ^4He coming from surrounding crustal rock and/or

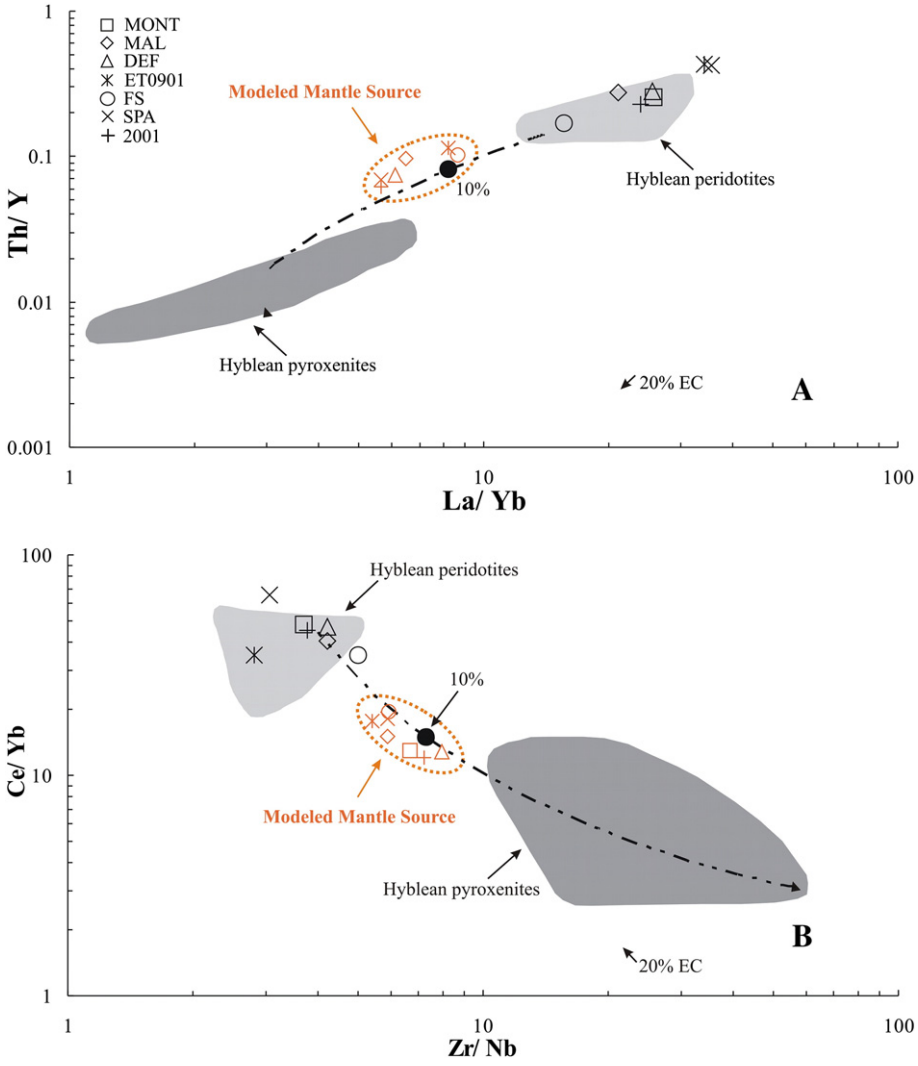

Fig. 11. Plots of Th/Y versus La/Yb (A) and Ce/Yb versus Zr/Nb (B) comparing whole-rock samples (symbols with black boundary) and recalculated compositions (symbols with orange boundary) of Etnean mantle source. The dashed black lines are the mixing curves between hypothetical peridotitic and pyroxenitic sources; numbers are the percentages of mixing. The dashed orange circle indicates the field of Etnean modeled mantle sources. The shaded gray areas are as in Fig. 4. EC as in Fig. 10.

an aged intrusive body could lower the R/Ra value of the reservoir by ~1 unit over a long timescale.

Regardless of which process is involved, our results suggest that magma with $^3He/^4He$ values of 6.6–6.8 Ra characterizes the crustal reservoirs below Mt. Etna, while the mantle source provides melts with values of about 7.6 Ra. This means that supply of ^4He into the ascending magma could have lowered the $^3He/^4He$ values of recent Etnean lavas. Thus, the rate of ascent and time of storage would be key parameters in controlling the $^3He/^4He$ values of a particular erupted lava sample. Considering that $^3He/^4He$ values for fluid inclusions in olivines from Etnean products are generally ≤7 Ra (Marty et al., 1994; Nuccio et al., 2008), it is likely that the SPA lava eruption, whose products have a $^3He/^4He$ value of 7.6 Ra, was characterized by a very rapid ascent and/or a short storage time in the magma reservoir, which prevented significant aging and/or crustal contamination.

6.4. A two-component mantle source evidenced by coupling between noble gases and trace elements

We can now integrate the information from modeling and comparisons with data of Hyblean xenoliths to constrain the structure and compositional features of Etnean mantle. Firstly, we recall some of the results obtained by Correale et al. (2012), who focused on the geochemical characteristics of the Hyblean mantle source. They identified (i) mantle heterogeneity, composed of a peridotitic (HIMU-like) and a pyroxenitic (DM-like) domain, and (ii) metasomatic events, characterized by pyroxenitic veins intruding into the peridotitic matrix. They coupled $^3He/^4He$ ratios with the trace elements Nd and Sm to model different degrees of metasomatism by mixing the two end-members. We adopted a similar approach by combining the results for noble gases and trace elements. Fig. 12 plots the $^3He/^4He$ values of Hyblean peridotites and pyroxenites versus the Zr/Nb ratio and Nd concentration (peridotitic end-member: $^3He/^4He = 7$ Ra, $He = 3 \times 10^{-13}$ mol/g; Zr = 6 ppm, Nb = 1.5 ppm and Zr/Nb = 4; pyroxenitic end-member: $^3He/^4He = 7.6$ Ra, $He = 1.02 \times 10^{-11}$ mol/g, Zr = 22.6 ppm, Nb = 0.4 ppm and Zr/Nb = 56), which clearly distinguishes the two Hyblean domains. The measured He and Nd concentrations and Zr/Nb ratios of the two end-members—used to calculate the mixing path—are the highest measured in pyroxenites and the lowest measured in peridotites (Correale et al., 2012). The mixing curve between the two Hyblean mantle end-members is strongly convex due to the large differences in He content between the two end-members. Finally, we plotted the modeled mantle

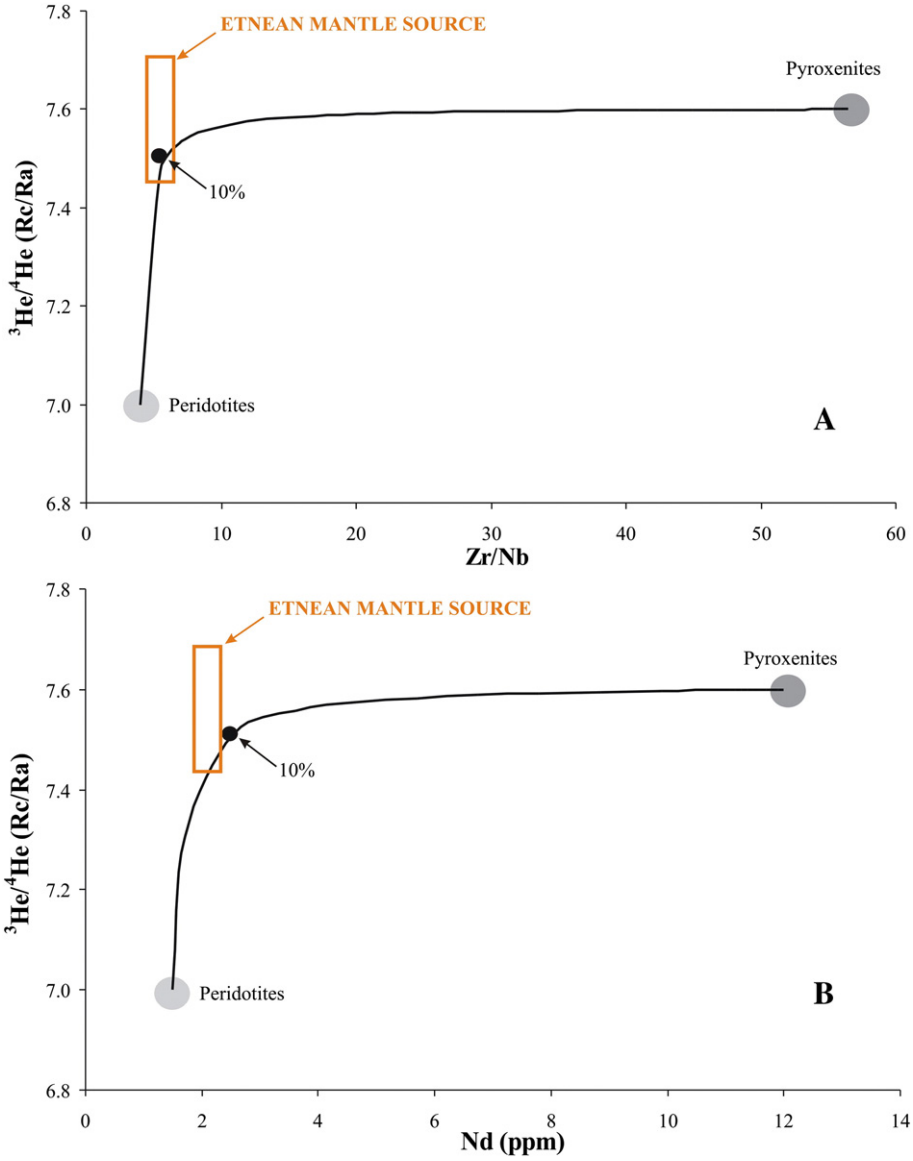

Fig. 12. Plots of $^3He/^4He$ (in Rc/Ra) versus Zr/Nb ratio (A) and $^3He/^4He$ (in Rc/Ra) versus Nd abundance (B). The curve describes a mixing trend between a peridotitic and pyroxenitic end members. Black symbols on the mixing curve indicate the percentage of pyroxenitic end-member. The orange rectangle indicates the modeled Etnean mantle source.

source of the Etnean magmas. The Nd, Zr and Nb concentrations for the Etnean source were calculated using the same procedure as for other investigated trace elements (see Section 6.1), whereas the $^3He/^4He$ value of the Etnean mantle source was that of SPA.

Fig. 12 shows that the Etnean source falls along the peridotite–pyroxenite mixing curve, and is therefore compatible with this process. The low Nd content (~2 ppm) typical of a peridotitic source is associated with the high $^3He/^4He$ value (i.e., 7.6 Ra) typical of a pyroxenitic mantle, highlighting the contribution of pyroxenitic veins to the source of Etnean magmas. Pyroxenitic metasomatism provides the strong fingerprint of He isotopes, but increases the concentrations of most trace elements only slightly, which therefore retain values closer to those of the peridotite layer. The mixing curve between the peridotitic and pyroxenitic end-members also allows evaluations of the amount of pyroxenitic melt involved in the generation of Etnean lava; this was found to be ~10% (Fig. 12), which is consistent with trace-element geochemistry. In plots of Zr/Nb versus Ce/Yb and Th/Y versus La/Yb (Fig. 11), the modeled Etnean mantle source has a mainly peridotitic nature but also a significant pyroxenitic contribution (~10%).

6.5. Inference on the origin of Etnean lavas: melting of a variably metasomatized mantle

The two-component mantle as discussed above would be able to produce the spectrum of mafic Etnean magmas with variable degrees of partial melting followed by variable degrees of melt crystallization (see Section 6.1). The degree of partial melting is highly variable over a relatively short timescale; that is, it increases from 1% for SPA to a maximum of 10% for FS over 11 ky, and decreases to 2% for products younger than 4 ky BP. However, changes induced by different degrees of batch melting cannot explain the geochemical watershed between pre- and post-1971 Etnean products (variations in K, Rb and Sr isotopes; Clocchiatti et al., 1988; Joron and Treuil, 1984). Indeed, the post-1971 samples, namely DEF and from the 2001 eruption, result from the same degree of melting of the mantle source with respect to the 1763 MONT eruption.

The large variations in the degree of mantle melting over a short time, as inferred from the samples measured by us, would require very rapid processes. Such a short timescale makes it difficult to propose the development of a thermal or baric transient at the mantle level,

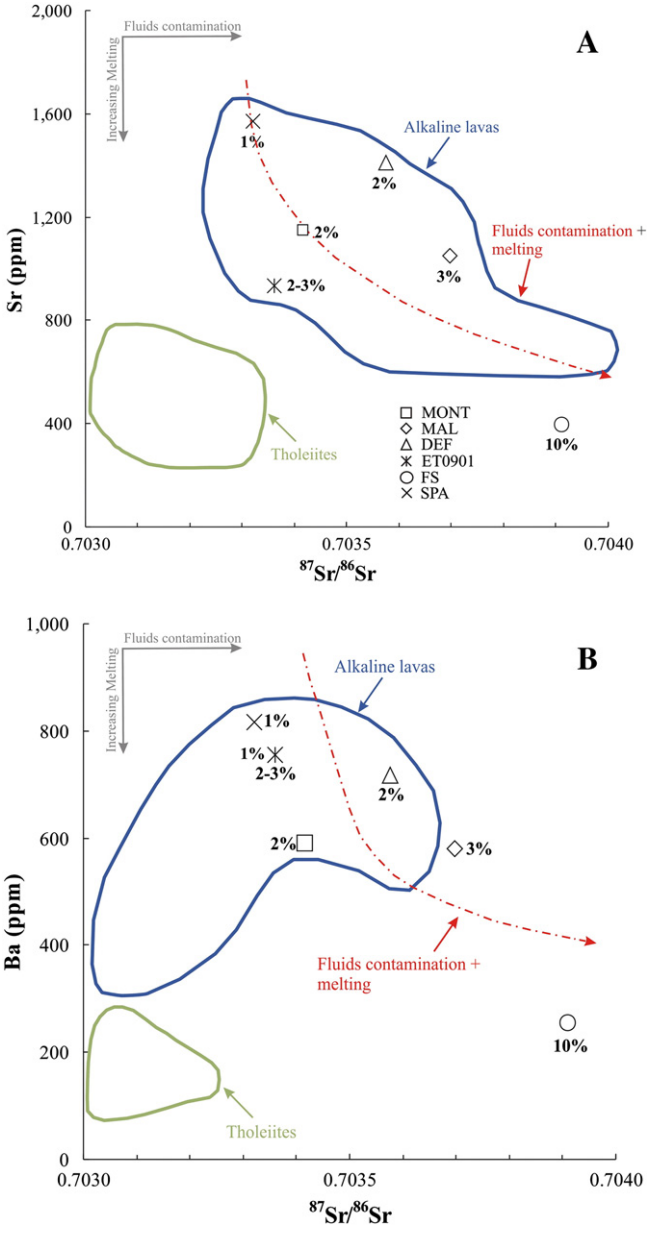

Fig. 13. Plots of Sr (A) and Ba (B) versus $^{87}Sr/^{86}Sr$. Colored fields are reported for comparison as in Fig. 3 (Armienti et al., 2004; Carter and Civetta, 1977; D'Orazio, 1993; Viccaro and Cristofolini, 2008). The black labels indicate the melting percentages estimated for each sample by MELTS code (see Section 6.1). The red dashed lines represent the variations of elemental Sr (A) and Ba (B) versus isotopic Sr due to the combined effects of mantle contamination by fluids and consequent partial mantle melting (see the text for further details).

since that would require a longer timescale. In accordance with our conclusion in Section 6.1, either temperature increase or depressurization (i.e., isobaric and isothermal melting, respectively) is therefore an unrealistic process for melt generation in the Etnean mantle source. Instead, consistent with our preferred flux melting model, it seems more likely that the variable degree of mantle melting is derived from the presence of heterogeneous fluids in the mantle source. A higher concentration of fluids in a local mantle portion would be responsible for a higher degree of partial melting. We therefore agree with the hypothesis of Viccaro and Cristofolini (2008) of a heterogeneous marble-cake mantle variably enriched in fluids derived from ancient subduction.

The interpretation of a variably metasomatized mantle has implications for trace elements that have an affinity for fluid phases (i.e., LILE). Recalling that our modeled Etnean mantle source was calculated using fluid immobile elements, its computed composition and degree of melting are reliable even if a metasomatic event was superimposed. With this in mind, we note that our samples show an increase in the degree of melting of more radiogenic (high $^{87}Sr/^{86}Sr$) magmas, but a progressive decrease in their LILE content (Fig. 13): FS and SPA, having the highest and lowest degrees of melting, respectively, display the most- and least-radiogenic compositions and the lowest and highest Sr contents, respectively. In contrast, we can expect that mantle portions most affected by metasomatic events will display a higher $^{87}Sr/^{86}Sr$ ratio and degree of melting, as well as a higher LILE content.

To investigate this inconsistency we evaluated the combined effects of metasomatism and mantle melting on magma geochemistry. We first simulated possible metasomatic events by mixing of the least-contaminated Etnean mantle source (i.e., SPA) with variable amounts of a metasomatic aqueous fluid. The Sr and Ba contents (45 ppm Sr and 9.2 ppm Ba) of the less-contaminated Etnean mantle portion are obtained from the SPA sample using the calculations in Section 6.1, whereas the isotopic Sr ratio ($^{87}Sr/^{86}Sr = 0.70333$) is that measured in the SPA sample. We assumed the metasomatic aqueous fluids to comprise 8000 ppm Sr and 5000 ppm Ba, which is compatible with the range estimated by Johnson et al. (2009) for a H_2O-rich subduction component of oceanic crust, and suggests a greater contribution of fluids from sediments (Lagatta, 2003) than from the oceanic crust (Staudigel et al., 1995). The assumed isotopic Sr ratio of the metasomatic fluid was $^{87}Sr/^{86}Sr = 0.709$, which reflects the simultaneous presence of altered oceanic crust (Staudigel et al., 1995) and sediment (Weldeab et al., 2002) components. The results of mixing provide the $^{87}Sr/^{86}Sr$ value and LILE composition of mantle portions that exhibit diverse extents of fluid contamination. We then associated with each of these contaminated mantle portions a melting percentage linked to the amount of added metasomatic H_2O, computed from a flux melting simulation (using the MELTS program; see Section 6.1), and we used the batch melting equation (see [1]) to calculate the LILE composition of the generated magma. Fig. 13 presents the results of these interacting processes, where the dashed red curve shows the variations of two LILE elements (Sr and Ba) versus $^{87}Sr/^{86}Sr$. Due to the uncertainty about the H_2O content from the subducted slab and the percentages of sediment and oceanic crust fluids involved in the subduction, some variations in the Sr-isotope marker and Sr and Ba concentrations of the fixed aqueous fluid end-member are possible, but they would not change the overall shape of the curve.

The calculations highlight that the LILE content in the produced melts critically depends on the degree of melting of the mantle. In fact, starting from the least-radiogenic Sr-isotope ratio of SPA ($^{87}Sr/^{86}Sr = 0.7033$), the addition of Sr and Ba at only a few ppm (by ~0.07 wt.% of the crustal fluid end-member) to the mantle would yield the most-enriched isotope composition of FS ($^{87}Sr/^{86}Sr = 0.7039$). At the same time, the addition of H_2O increases the degree of melting from 1% (as estimated for SPA) to 10% (for FS). An increase in the melting percentage causes a dramatic drop in the Sr and Ba contents in the produced melts (of about 700 and 500 ppm, respectively). Increases in Sr and Ba of only a few ppm (Table 3) in the source due to the addition of metasomatic crustal fluids could therefore be considered negligible. Thus, the differences in enrichment in LILE between the samples are mainly due to the variable percentages of source melting. In other words, although SPA represents the least-contaminated sample for Sr and Nd isotopes (i.e., the lowest $^{87}Sr/^{86}Sr$ ratio), it shows the highest LILE concentration due to the low melting percentages involved in its generation. Paradoxically, the absolute contents of fluid mobile elements in our lavas do not reflect the amount of metasomatic fluid added to the mantle source, but rather the degree of melting. This modeled process explains the inverse relationship that we observe between Sr (and Ba) and $^{87}Sr/^{86}Sr$ (red curve in Fig. 13).

A final aspect of our model of a mantle heterogeneously enriched by fluid phases involves the combined interpretation of He and Sr isotope

Table 3
Variations of elemental Sr and Ba versus isotopic Sr due to metasomatism (marked by circles) and partial melting (marked by stars) of the source.

	H_2O(wt%) (crustal fluids)	$^{87}Sr/^{86}Sr$	Sr *(ppm)	Ba*(ppm)		Sr°(ppm)	Ba°(ppm)
Increasing metasomatism	0,015	0,7033	45,07	9,25	Increasing partial melting		
		0,7034	45,35	9,45		1523	834
	0,030	0,7036	46,04	9,95		1163	467
	0,075	0,7038	47,09	10,70		954	342
		0,7040	47,78	11,20		796	271
	0,180	0,7046	50,56	13,19		598	215
		0,7061	58,91	19,18		446	189

ratios. The $^3He/^4He$ values are highest for SPA and MAL, but these lavas show the lowest and highest $^{87}Sr/^{86}Sr$ ratios, respectively (see Figs. 7 and 8), thus indicating that the two isotopic systems are decoupled and that no clear relationship exists between mantle metasomatism by a crustal-like contaminant and He isotope values. Only the SPA sample, with the highest $^3He/^4He$ ratio and lowest $^{87}Sr/^{86}Sr$ among our data, is consistent with our mantle model. Therefore, the decoupling between He and Sr requires the presence of additional processes in the crustal reservoirs, as suggested by comparison of the Rc/Ra values of our lavas with those of volcanic gas discharges (Section 6.3). Consequently, magma aging and crustal contamination are probably the main mechanisms responsible for lowering the He-isotope ratio of the magmas stored in the crust, due to the addition of radiogenic ^4He (see Section 6.3).

7. Final remarks

We have presented the results of geochemical study of selected primitive, post-15 ky lavas and tephra from Mt. Etna volcano in order to characterize its mantle source. The integration of petrological and geochemical features suggests that the Etnean magmatism is linked with the older mafic magmatism of the Hyblean Plateau. In particular, our data suggest firstly that primitive magmas from Mt. Etna originate from different degrees of partial melting of a mantle source that is very similar to the Hyblean one in terms of its composition of trace elements and Sr, Nd and He isotopes. This common source is characterized by a peridotitic component metasomatized by former primitive melts (clinopyroxenitic or clinopyroxene-rich veins). The pyroxenitic end-member contributes about 10% melt to the Etnean lavas. Ratios of highly incompatible, immobile, trace elements primarily carry information about the peridotitic component; in contrast, He isotopes, showing a higher sensitivity to the effect of metasomatic mixing, exhibit typical pyroxenitic values. However, this is restricted to those samples not affected by the contribution of crustal radiogenic He after the melt has been produced. Such modification of the He-isotope ratio explains the absence of a correlation between He isotopes and Sr and Nd isotopes in many samples. Secondly, spatially variable contents of crustal-type fluids—probably inherited from subduction—characterize the mantle source of Mt. Etna, which is therefore strongly heterogeneous. Such spatial heterogeneity is probably also responsible for the different degrees of melting estimated for the studied lavas. While the Sr- and Nd-isotope compositions are the best markers of such fluid metasomatism, the trace-element contents are chiefly controlled by the degree of partial melting of the mantle source.

Supplementary data to this article can be found online at http://dx.doi.org/10.1016/j.lithos.2013.10.038.

Acknowledgments

We wish to thank L. Brusca and S. Bellomo for their support during the analysis of trace elements. Thanks are due to M. Coltelli and P. Del Carlo for many helpful discussions on tephrostratigraphy of Mt. Etna. We are grateful to Editor-in-Chief A. Kerr, Prof. D. Kamenetsky and two anonymous reviewers for their constructive criticism that significantly improved the paper. This work is part of the PhD thesis of Alessandra Correale financially supported by the Università degli Studi di Palermo.

References

Armienti, P., Innocenti, F., Petrini, R., Pompilio, M., Villari, L., 1988. Sub-aphyric alkali basalt from Mt Etna: inferences on the depth and composition of the source magma. Rendiconti della Societa Italiana di Mineralogia e Petrologia 43, 877–891.
Armienti, P., Clocchiatti, R., D'Orazio, M., Innocenti, F., Petrini, R., Pompilio, M., Tonarini, S., Villari, L., 1994. The long-standing 1991–1993 Mount Etna eruption: petrography and geochemistry of lavas. Acta Vulcanologica 4, 15–28.
Armienti, P., Tonarini, S., D'Orazio, M., Innocenti, F., 2004. Genesis and evolution of Mt Etna alkaline lavas: petrological and Sr–Nd–B isotope constraints. Periodico di Mineralogia 73, 29–52.
Armienti, P., Tonarini, S., Innocenti, F., D'Orazio, M., 2007. Mount Etna pyroxene as tracer of petrogenetic processes and dynamics of the feeding system. In: Beccaluva, L., Bianchini, G., Wilson, M. (Eds.), Volcanism in the Mediterranean and surrounding regions. Geological Society of America, Special Paper, 418, pp. 265–276.
Beccaluva, L., Siena, F., Coltorti, M., Digrande, A., Lo Giudice, A., Macciotta, G., Tassinari, R., Vaccaro, C., 1998. Nephelinitic to tholeiitic magma generation in a transtensional tectonic setting: an integrated model for the Iblean vulcanism, Sicily. Journal of Petrology 39, 1547–1576.
Bianchini, G., Yoshikawa, M., Sapienza, G.T., 2010. Comparative study of ultramafic xenoliths and associated lavas from South-Eastern Sicily: nature of the lithospheric mantle and insights on magma genesis. Mineralogy and Petrology 98, 111–121.
Branca, S., Coltelli, M., Groppelli, G., 2011a. Geological evolution of a complex basaltic stratovolcano: Mount Etna, Italy. Italian Journal of Geosciences 130, 306–317.
Branca S., Coltelli M., Groppelli G., Lentini F., 2011b. Geological map of Etna volcano, 1:50,000 scale. Italian Journal of Geosciences 130, 265–291.
Burnard, P.G., Hu, R., Turner, G., Bi, X.W., 1999. Mantle, crustal and atmospheric noble gases in Ailaoshan Gold deposits, Yunnan Province, China. Geochimica et Cosmochimica Acta 63, 1595–1604.
Cadoux, A., Blichert-Toft, J., Pinti, D.L., Albarède, F., 2007. A unique lower mantle source for Southern Italy volcanics. Earth and Planetary Science Letters 259, 227–238.
Caracausi, A., Favara, R., Giammanco, S., Italiano, F., Paonita, A., Pecoraino, G., Rizzo, A., 2003. Mount Etna: geochemical signals of magma ascent and unusually extensive plumbing system. Geophysical Research Letters 30. http://dx.doi.org/10.1029/2002GL0115463.
Carter, S.R., Civetta, L., 1977. Genetic implications of the isotope and trace element variations in the eastern Sicilian volcanics. Earth and Planetary Science Letters 36, 168–180.
Clocchiatti, R., Joron, J.L., Treuil, M., 1988. The role of selective alkali contamination in the evolution of recent historic lavas of Mt Etna. Journal of Volcanology and Geothermal Research 34, 241–249.
Clocchiatti, R., Condomines, M., Guénot, N., Tanguy, J.C., 2004. Magma changes at Mount Etna: the 2001 and 2002–2003 eruptions. Earth and Planetary Science Letters 226, 397–414.
Coltelli, M., Del Carlo, P., Pompilio, M., Vezzoli, L., 1998. Discovery of a Plinian basaltic eruption of Roman age at Etna volcano, Italy. Geology 26, 1095–1098.
Coltelli, M., Del Carlo, P., Vezzoli, L., 2000. Stratigraphic constrains for explosive activity in the last 100 ka at Etna volcano, Italy. International Journal of Earth Sciences 89, 665–677.
Coltelli, M., Del Carlo, P., Pompilio, M., Vezzoli, L., 2005. Explosive eruptions of a picrite: the 3930 BP subplinian eruption of Etna volcano (Italy). Geophysical Research Letters 32, L23307. http://dx.doi.org/10.1029/2005GL024271.
Condomines, M., Tanguy, J.C., Kieffer, G., Allegre, C.J., 1982. Magmatic evolution of a volcano studied by 230Th–238U disequilibrium and trace element systematics: the Etna case. Geochimica et Cosmochimica Acta 46, 1397–1416.
Condomines, M., Bouchez, R., Ma, J.L., Tanguy, J.C., Amosse, J., Piboule, M., 1987. Short-lived radiactive disequilibria and magma dynamics in Etna volcano. Nature 325, 607–609.
Correale, A., Martelli, M., Paonita, A., Rizzo, A., Brusca, L., Scribano, V., 2012. New evidences of mantle heterogeneity beneath the Hyblean Plateau (southeast Sicily, Italy) as inferred from noble gases and geochemistry of ultramafic xenoliths. Lithos 132–133, 70–81.
Corsaro, R.A., Cristofolini, R., 1997. Geology, geochemistry and mineral chemistry of tholeiitic to transitional Etnean magmas. Acta Vulcanologica 9, 55–66.
Corsaro, R.A., Cristofolini, R., 2000. Subacqueous volcanism in the Etnean area: evidence for hydromagmatic activity and regional uplift inferred from the Castle Rock of Acicastello. Journal of Volcanology and Geothermal Research 95, 209–225.
Corsaro, R.A., Pompilio, M., 2004. Dynamics of magmas at Mount Etna. Mount Etna: volcano laboratory. Bonaccorso, Calvari, Del Negro, Falsaperla. AGU Geophysical Monograph Series, 143, pp. 91–110.
Corsaro, R.A., Miraglia, L., Pompilio, M., 2006. Petrologic evidence of a complex plumbing system feeding the July–August 2001 eruption of Mt. Etna, Sicily, Italy. Bulletin of Volcanology 69, 401–421.
Corsaro, R.A., Métrich, N., Allard, P., Andronico, D., Miraglia, L., Fourmentraux, C., 2009. The 1974 flank eruption of Mount Etna: an archetype for deep dike-fed eruptions at basaltic volcanoes and a milestone in Etna's recent history. Journal of Geophysical Research 114, B07204. http://dx.doi.org/10.1029/2008JB006013.
Coulson, I.M., Stuart, F.M., MacLean, N.J., 2011. Assessing the link between mantle source and sub-volcanic plumbing in the petrology of basalts from 2001 and 2002/2003

eruptions of Mount Etna, Sicily: evidence from geochemical and helium isotope data. Lithos 123, 254–261.
Cristofolini, R., Corsaro, R.A., Ferlito, C., 1991. Variazioni petrochimiche nella successione etnea: un riesame in base ai nuovi dati da campioni di superficie e da sondaggi. Acta Vulcanologica 1, 25–37.
D'Orazio, M., 1993. Natura ed evoluzione delle vulcaniti dell'Etna e loro relazioni con il magmatismo Ibleo. (PhD thesis) Università di Pisa.
D'Orazio, M., Tonarini, S., Innocenti, F., Pompilio, M., 1997. The northern Valle del Bove volcanic succession (Mt Etna Sicily): petrography, geochemistry and Sr–Nd isotope data. Acta Vulcanologica 9 (1), 69–79.
De Beni, E., Branca, S., Coltelli, M., Groppelli, G., Wijbrans, J.R., 2011. $^{40}Ar/^{39}Ar$ isotopic dating of Etna volcanic succession. Italian Journal of Geosciences 130, 292–305.
De Gori, P., Chiarabba, C., Patanè, D., 2005. Qp structure of Mount Etna: constraints for the physics of the plumbing system. Journal of Geophysical Research 110, B05303. http://dx.doi.org/10.1029/2003JB002875.
Del Carlo, P., Vezzoli, L., Coltelli, M., 2004. Last 100 ka tephrostratigraphic record of Mount Etna. In Mt Etna: volcano laboratory. Geophysical Monograph Series 143, 77–89.
Di Renzo, V., Di Vito, M.A., Arienzo, I., Carandente, A., Civetta, L., D'Antonio, M., Giordano, F., Orsi, G., Tonarini, S., 2007. Magmatic history of Somma–Vesuvius on the basis of new geochemical and isotopic data from a deep borehole (Camaldoli della Torre). Journal of Petrology 48, 753–784.
Doglioni, C., Innocenti, F., Mariotti, G., 2001. Why Mt Etna? Terra Nova 13, 25–31.
Finocchiaro, S., 1995. Petrology of the succession of Etnean lavas with reference to ancient alkaline lavas. Plinius 12, 73–78.
Ghiorso, M.S., Sack, R.O., 1995. Chemical mass transfer in magmatic processes IV. A revised and internally consistent thermodynamic model for interpolation and extrapolation of liquid–solid equilibria in magmatic systems at elevated temperatures and pressures. Contributions to Mineralogy and Petrology 119, 197–212.
Giggenbach, W.F., Sano, Y., Wakita, H., 1993. Isotopic composition of helium, and CO_2 and CH_4 contents in gas produced along the New Zealand part of a convergent plate boundary. Geochimica et Cosmochimica Acta 57, 3427–3455.
Goldstein, S.L., Deines, P., Oelkers, E.H., Rudnick, R.L., Walter, L.M., 2003. Standards for publication of isotope ratio and chemical data in chemical geology. Chemical Geology 202, 1–4.
Hilton, D.R., Barling, J., Wheller, G.E., 1995. Effect of shallow level contamination on the helium isotope systematics of ocean–island–lavas. Nature 373, 330–333.
Hilton, D.R., Fischer, T.P., Marty, B., 2002. Noble gases and volatile recycling at subduction zones. In: Porcelli, D.P., Ballentine, C.J., Wieler, R. (Eds.), Noble Gases in Geochemistry and Cosmochemistry: Reviews in Mineralogy and Geochemistry, 47, pp. 319–370.
Johnson, E.R., Wallace, P.J., Delgado Granados, H., Manea, V.C., Kent, A.J.R., Bindeman, I., Donegan, C.S., 2009. Subduction-related volatile recycling and magma generation beneath Central Mexico: insights from melt inclusions, oxygen isotopes and geodynamic models. Journal of Petrology 50 (9), 1729–1764. http://dx.doi.org/10.1093/petrology/egp051.
Joron, J.L., Treuil, M., 1984. Etude geochimique et pétrogenèse des laves de l'Etna. Bulletin of Volcanology 47, 1125–1144.
Kamenetsky, V.S., Clocchiatti, R., 1996. Primitive magmatism of Mt. Etna: insights from mineralogy and melt inclusions. Earth and Planetary Science Letters 142, 553–572.
Kamenetsky, V.S., Pompilio, M., Métrich, N., Sobolev, A., Kuzmin, D.V., Thomas, R., 2007. Arrival of extremely volatile-rich high-Mg magmas changes explosivity of Mount Etna. Geological Society of America 35, 255–258.
Lagatta, A., 2003. Arc Magma Genesis in the Eastern Mexican Volcanic Belt. (Ph.D. thesis) Columbia University, New York.
Le Maitre, R.W. (Ed.), 2002. Igneous rocks. A classification and glossary of terms, 2nd ed. Recommendations of the IUGS Subcomission on the Systematics of Igneous Rocks. Cambridge University Press, p. 236.
Liotta, M., Rizzo, A., Paonita, A., Caracausi, A., Martelli, M., 2012. Sulfur isotopic compositions of fumarolic and plume gases at Mt. Etna (Italy) and inferences on their magmatic source. Geochemistry, Geophysics, Geosystems 13. http://dx.doi.org/10.1029/2012GC004118.
Lux, G., 1987. The behavior of noble gases in silicate liquids: solution, diffusion, bubbles and surface effects, with applications to natural samples. Geochimica et Cosmochimica Acta 51, 1549–1560.
Marty, B., Trull, T., Lussiez, P., Basile, I., Tanguy, J.C., 1994. He, Ar, O, Sr and Nd isotope constraints on the origin and evolution of Mount Etna magmatism. Earth and Planetary Science Letters 126, 23–39.
Mattia, M., Patanè, D., Aloisi, M., Amore, M., 2007. Faulting on the western flank of Mt Etna and magma intrusions in the shallow crust. Terra Nova 19, 89–94. http://dx.doi.org/10.1111/j1365-3121.2006.00724.x.
Métrich, N., Allard, P., Spilliaert, N., Andronico, D., Burton, M., 2004. 2001 flank eruption of the alkali and volatile-rich primitive basalt responsible for Mount Etna's evolution in the last three decades. Earth and Planetary Science Letters 228, 1–17.
Michaud, V., 1995. Crustal xenoliths in recent hawaiites from Mount Etna, Italy—evidence for alkali exchanges during magma–wall rock interaction. Chemical Geology 122, 21–42.
Miraglia, L., 2002. Evidence for heterogeneous magmas in the feeding system of the 1763 "La Montagnola" eruption at Mount Etna. Plinius 27, 108–112.
Nuccio, P.M., Paonita, A., Rizzo, A., Rosciglione, A., 2008. Elemental and isotope covariation of noble gases in mineral phases from Etnean volcanics erupted during 2001–2005, and genetic relation with peripheral gas discharges. Earth and Planetary Science Letters 272, 683–690.
Paonita, A., Caracausi, A., Marziano-Iacono, G., Martelli, M., Rizzo, A., 2012. Geochemical evidences for mixing between fluids exsolved at different depths in the magmatic system of Mt Etna (Italy). Geochimica et Cosmochimica Acta 84, 380–394.
Patanè, D., Barberi, G., Cocina, O., De Gori, P., Chiarabba, C., 2006. Time-resolved seismic tomography detects magma intrusions at Mt. Etna. Science 313, 821–823.
Peccerillo, A., 2005. Plio-Quaternary Volcanism in Italy. Springer.
Perinelli, C., Sapienza, G.T., Armienti, P., Morten, L., 2008. Metasomatism of the upper mantle beneath the Hyblean Plateau (Sicily): evidence from pyroxenes and glass in peridotite xenoliths. London Geological Society, Special Publication 293, 197–221.
Rittman, A., 1965. Notizie sull'Etna. Nuovo Cimento 3 (I), 1117–1123 (Suppl.).
Rotolo, S.G., Castorina, F., Cellura, D., Pompilio, M., 2006. Petrology and geochemistry of submarine volcanism in the Sicily Channel Rift. Journal of Geology 114, 355–365.
Sapienza, G., Scribano, V., 2000. Distribution and representative whole rock chemistry of deep-seated xenoliths from the Iblean Plateau, South-Eastern Sicily, Italy. Periodico di Mineralogia 69, 185–204.
Sapienza, G., Hilton, D.R., Scribano, V., 2005. Helium isotopes in peridotite mineral phases from Hyblean Plateau xenoliths (southeastern Sicily, Italy). Chemical Geology 219, 115–129.
Shaw, A.M., Hilton, D.R., Fisher, T.P., Walker, J.A., De Leeuw, G.A.M., 2006. Helium isotope variations in mineral separates from Costa Rica and Nicaragua. Assessing crustal contribution, timescale variations and diffusion related mechanism. Chemical Geology 230, 124–139.
Spence, A., Downes, H., 2011. A chemostratigraphic investigation of the prehistoric Vavalaci lava sequence on Mount Etna: simulating borehole drilling. Lithos 125, 423–433.
Staudigel, H., Davies, G.R., Hart, S.R., Marchant, K.M., Smith, B.M., 1995. Large-scale isotopic Sr, Nd and O isotopic anatomy of altered oceanic crust DSDP/ODP sites 417/418. Earth and Planetary Science Letters 130, 169–185.
Sturiale, C., 1970. La singolare eruzione dell'Etna del 1763 "La Montagnola". Bollettino Mineralogia Rendiconti della Società Italiana di Mineralogia e Petrologia 26, 314–351.
Sun, S., McDonough, W.F., 1989. Chemical and isotopic systematics of ocean basalts: implications for mantle composition and processes. In: Saunders, A.D., Norry, M.J. (Eds.), Magmatism in the ocean basins. Geological Society Special Publication, pp. 313–345.
Tanguy, J.C., 1978. Tholeitic basalt magmatism of Mount Etna and its relations with the alkaline series. Contributions to Mineralogy and Petrology 66, 51–67.
Tanguy, J.C., 1980. L'Etna: Etude pétrologique et paleomagnetique implications volcanologiques. (These de Doctorat d'état) , 6. Université Pierre et Marie Curie, Paris.
Tanguy, J.C., Condomines, M., Kieffer, G., 1997. Evolution of Mount Etna magma: constraints on the present feeding system and eruptive mechanism. Journal of Volcanology and Geothermal Research 75, 221–250.
Tonarini, S., D'Orazio, M., Armienti, P., Innocenti, F., Scribano, V., 1996. Geochemical features of Eastern Sicily lithosphere as probed by Hyblean xenoliths and lavas. European Journal of Mineralogy 5, 1153–1174.
Tonarini, S., Armienti, P., D'Orazio, M., Innocenti, F., 2001. Subduction-like fluids in the genesis of the Mt Etna magmas: evidence from boron isotopes and fluid mobile elements. Earth and Planetary Science Letters 5989, 1–13.
Viccaro, M., Cristofolini, R., 2008. Nature of mantle heterogeneity and its role in the short-term geochemical and volcanological evolution of Mt Etna (Italy). Lithos 105, 272–288.
Viccaro, M., Ferlito, C., Cortesogno, L., Cristofolini, R., Gaggero, L., 2006. Magma mixing during the 2001 event at Mount Etna (Italy): effect on the eruptive dynamics. Journal of Volcanology and Geothermal Research 149, 139–159.
Viccaro, M., Nicotra, E., Millar, I., Cristofolini, R., 2011. The magma source at Mount Etna volcano: perspective from the Hf isotope composition of historic and recent lavas. Chemical Geology 281, 343–351.
Weldeab, S., Emeis, K.C., Hemleben, C., Siebel, W., 2002. Provenance of lithogenic surface sediments and pathways of riverine suspended matter in the Eastern Mediterranean Sea: evidence from $^{143}Nd/^{144}Nd$ and $^{87}Sr/^{86}Sr$ ratios. Chemical Geology 186, 139–149.
White, W.M., 2007. Geochemistry. John-Hopkins University Press.
Wilson, M., 1989. Igneous Petrogenesis. Unwin Hyman, London.